CALIFORNIA STATE UNIVERSITY, NORTHRIDGE

Spatio-Temporal Patterns of Lower Arc Cooling and Metamorphism, Northern Fiordland, New Zealand

A thesis submitted in partial fulfillment of the requirements
for the degree of Master of Science in Geological Sciences

By

Samantha Kelly Gebauer

May 2016

The thesis of Samantha Kelly Gebauer is approved by:

_____	_____
Dr. Robinson Cecil	Date
_____	_____
Dr. Harold Stowell	Date
_____	_____
Dr. Joshua Schwartz, Chair	Date

California State University, Northridge

ACKNOWLEDGEMENTS

I would like to first thank Dr. Joshua Schwartz for his inexhaustible dedication to my project and as well as my success as a graduate student. He has been the best resource I could have asked for during the two years of my master's degree. I feel fortunate to have been given the opportunities he has given me during my graduate career. Thank you to Dr. Robinson Cecil and Dr. Harold Stowell for serving on my thesis committee and providing me valuable insight and edits for the duration of this thesis project. Thank you to Dr. Elena Miranda, Dr. Doug Yule, Dr. Richard Heermance, Dr. Kathleen Marsaglia, Dr. Keith Klepeis, Dr. Nick Mortimer, Dr. Matt Coble, Dr. Andrew Kylander-Clark, and all the other geoscientists who have helped provide me with preparing samples, running data analyses, processing data, and providing me insights necessary to help in completing this thesis.

I want to especially thank my colleague Meghann Decker for all of her advice, support, critiques, humor, and wisdom over the course of our respective Fiordland projects and beyond. Thank you also to my fellow students John Wiesenfeld, Brian Lee Clements, Jeffery Joseph III, Hannah Shamloo, and everyone else in the department who has provided insight, edits, assistance, and moral support during the course of this project.

Many thanks also to the CSUN Department of Geological Sciences, the CSUN Department of Graduate Studies, and the National Science Foundation for the financial support that made this project possible.

Finally, thank you to my closest friends Maureen Darcy, Paul Schlesinger, Mallory Montgomery, Ben Bradley, Suzanne Darcy, Dan McCarty, and Kelsey

O’Connor for their unconditional support and love. And infinite thanks to my parents, Jennifer and David Cobert, and my grandparents, Stan and Elizabeth Meader, for everything they have done and continue to do for me.

TABLE OF CONTENTS

LIST OF FIGURES

LIST OF TABLES

ABSTRACT

Spatio-Temporal Patterns of Lower Arc Cooling and Metamorphism, Northern Fiordland, New Zealand

By

Samantha Kelly Gebauer

Master of Science in Geological Sciences

The exhumed root of the Triassic to Early Cretaceous continental arc in Fiordland, New Zealand preserves a record of deep crustal arc processes during and following high-flux magmatism from c. 124-115 Ma. We present new LASS-ICP-MS and SHRIMP-RG $^{206}Pb/^{238}U$ dates, as well as Ti-in-zircon and Zr-in-titanite temperatures for metamorphic zircon and titanite in order to (1) reconstruct the thermal history of northern Fiordland, and (2) illuminate spatio-temporal patterns in arc root metamorphism. Samples were collected over ~50 km along an arc-parallel transect from George Sound (~8 kbar) to Milford Sound (~16 kbar) in order to understand the thermal evolution of the arc as a function of paleocrustal depth.

Rims that grew on zircon in samples from the Arthur River Complex indicate that Early Cretaceous metamorphism initiated at 134.9 ± 3.1 Ma (T = 720°C) and lasted until 126.5 ± 2.7 Ma (T = 700 °C). Subsequent granulite-facies metamorphic zircon growth occurred from 121.3 ± 1.6 to 116.0 ± 2.3 Ma in Bligh and George Sounds at 830-700°C. These dates and temperatures overlap with existing garnet Sm-Nd dates from the Pembroke granulite (Milford Sound) and likely reflect heating associated with deep

crustal emplacement of the Western Fiordland Orthogneiss from c. 125-115 Ma during the final stages of Median Batholith magmatism.

Titanite LASS chronology of metasedimentary rocks shows complex spatio-temporal patterns that reveal multiple pulses of titanite growth and/or recrystallization. East of Sutherland Sound, titanites yield a date of 120.6 ± 4.4 Ma and a Zr-in-titanite temperature of 765°C, which is similar to metamorphic zircon results in the region. At George Sound, titanites yield a date of 112.0 ± 2.4 Ma and a temperature of 760°C which overlaps with values reported in central Fiordland from Caswell to Breaksea Sounds. Younger dates of 104.8 ± 1.6 and 94.0 ± 2.3 Ma also occur in Bligh and George Sounds, and yield temperatures of 930 and 840°C, respectively. These dates and temperatures indicate that titanite growth and/or recrystallization occurred during multiple pulses of lower crustal heating which we speculate may have resulted from either lithospheric thinning related to extension and/or episodic foundering of a high-density arc root produced during the arc flare-up event.

1. INTRODUCTION

Continental arcs are the primary locations on Earth where continental crust is generated and plays an important role in the differentiation and modification of crust through time (Dufek and Bergantz, 2005; Lee, 2014). The evolution and refinement of continental crust in arcs is closely related to the thermal structure of the arc which to a first order controls processes such as fractional crystallization, assimilation, and partial melting (REFs). As magmatic arcs, particularly Cordilleran arcs, are inherently regions of high heat flow where thermal energy is transferred from the mantle to the surface by conductive and advective transport of melts and fluids; their thermal budgets are controlled primarily by magma input into the crust from the underlying mantle (i.e., mantle power: de Silva et al., 2015). The existing thermal structure, as well as tectonic processes (e.g., lithospheric thickening/thinning) and non-tectonic processes also play important roles in controlling heat transfer from the mantle to the surface (Lee, 2014). Thus, understanding the interplay between magmatic, metamorphic, and tectonic processes is essential in understanding timescales and processes of continental crust generation and refinement in continental arcs.

The lower crust in arcs has long been recognized as an important 'factory' for continental crust construction and refinement. Hildreth and Moorbath, 1988 proposed that much of the geochemical diversity in arcs is developed in deep crustal zones of mixing, assimilation, storage, and homogenization, or MASH zones (see also 'hot zones' in Annen et al., 2006). Numerical models predict that deep crustal MASH zone to be an area of re-melting as well as high heat flow (Dufek and Bergantz, 2005). Since the lower crust is a key location where mantle-derived melts accumulate and are stored, understanding 1)

the timescale over which lower arc crust remains hot (> 700 °C), and 2) how those elevated temperatures influence the processes that control continental crust generation through time can provide insights into the evolution of arc systems (Hildreth and Moorbath, 1988; Daczko et al., 2005; Dufek and Bergantz, 2005). To investigate these questions, we examine the exhumed, tilted root of the Triassic to Early Cretaceous continental arc exposed in northern Fiordland, South Island, New Zealand, which preserves a record of deep crustal arc processes that operated prior to, during, and following a period of high-flux magmatism from c. 124-115 Ma (Figure 1) (Mattinson et al., 1986; Hollis et al., 2003; Hollis et al., 2004; Klepeis et al., 2003; Klepeis et al., 2007; Allibone et al., 2009).

Previous thermochronologic work in central Fiordland has documented protracted heating (T > 750°C) during and following the emplacement of the Western Fiordland Orthogneiss (WFO) into orthogneiss and paragneiss basement lasting over a period of longer than 15 Ma (Figure 1) (Hollis et al., 2004; Flowers et al., 2005; Schwartz et al., in press). Prolonged heating (>15 Ma) in central Fiordland resulted in a weak, hot lower crust which accommodated lower crustal extension in ductile shear zones that led to extensional orogenic collapse (e.g., Doubtful Sound Shear Zone; Figure 1) (Klepeis et al., 2003; Klepeis et al., 2007; Allibone et al., 2009; Stowell et al., 2014; Schwartz et al., in press).

In contrast to central Fiordland, previous studies have proposed that the lower crust in northern Fiordland cooled rapidly and was comparatively strong due to a lack of comparable observed extensional features, as well as cold (T = 650-700°C) by c. 116 Ma (Gibson and Ireland, 1995; Daczko et al., 2002; Klepeis et al., 2004; Klepeis et al., 2007).

In northern Fiordland, geochronologic data from Daczko et al. (2002) suggests rapid cooling of the lower crustal Arthur River Complex occurred in < 20 Ma due to its juxtaposition with cold upper crustal regions of the Median Batholith during tectonic burial (Figure 1). Additionally, one titanite date from the Arthur River Complex in Milford Sound was interpreted to reflect rapid cooling in the north to 600-650 °C by c. 120 Ma (Figure 1) (Flowers et al., 2005). However, elevated temperatures (c. 850 °C) recorded in Sm-Nd garnet dates from Pembroke Valley in Milford Sound are synchronous with plutonism, heating, and partial melting from 130 to 115 Ma (Figure 1) (Stowell, pers. comm..; Stowell et al., 2010). Two Sm-Nd garnet dates < 110 Ma (c. 109, garnet rim and c. 94 Ma, garnet reaction zone) from the same area further imply sustained heating resulting in either diffusive loss of radiogenic Nd and/or new garnet growth (Stowell et al., 2010). These results imply a prolonged period of lower crustal heating for 20-30 Ma and contradict earlier titanite cooling ages and arguments for a cold lower crust (Stowell et al., 2010).

We present new zircon and titanite thermochronology to 1) reconstruct the thermal history of the lower crust exposed in northern Fiordland, and 2) document timescales and duration of lower crustal metamorphism and cooling. Further, data are used to provide insights into processes in the MASH zone regarding continental crust generation and evolution, and may be applicable toward the study of other, less well-exposed Cordilleran-type arc systems. Together, our zircon and titanite data reveal that elevated temperatures (920 – 690 °C) persisted in the lower crust in northern Fiordland for over 40 Ma from 135 to 94 Ma. The timescale and temperatures are similar to those observed in central Fiordland and contrary to previous observations and interpretations.

Unlike central Fiordland, northern Fiordland lacks extensional features suggesting that thermal heating alone did not lead to strain localization during extensional orogenic collapse.

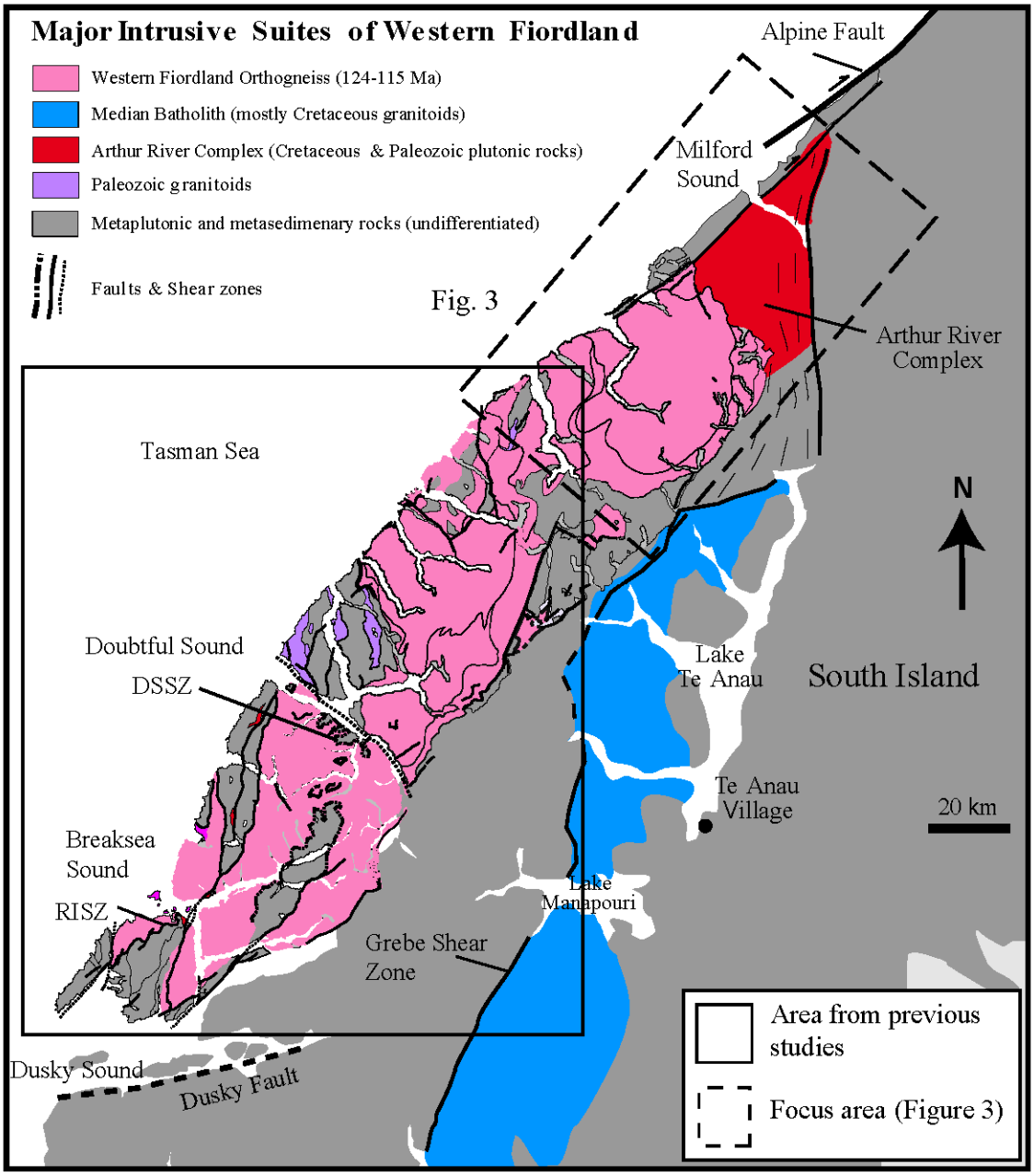

Figure 1: Simplified geologic map of central and northern Fiordland (after Allibone et al., 2009). Focus area in northern Fiordland indicated by dashed box; focus area of previous studies in central Fiordland indicated by solid box (see Figure 3 for detailed geologic map and sample locations). DSSZ = Doubtful Sound Shear Zone; RISZ = Resolution Island Shear Zone.

2. GEOLOGIC BACKGROUND

2.1 Tectonic history of Zealandia

The microcontinent Zealandia, of which New Zealand is a subaerial component, preserves a history of Mesozoic convergence and extension at the margin of the supercontinent Gondwana (Flowers et al., 2005; Mortimer, 2008). During the Late Paleozoic to Mesozoic, the Gondwana continental margin was dominated by convergent tectonics comprising multiple subduction zones and arc systems (Laird and Bradshaw, 2004). Zealandia was part of the Pacific-facing continental margin of Gondwana, bordering present-day Antarctica and Australia until the late Cretaceous (Figure 2). During the Late Cretaceous, the dominant tectonic regime in this area changed from convergent margin tectonics and arc magmatism to that of extension (Laird and Bradshaw, 2004; Mortimer, 2008).

The exact timing and processes that changed the tectonic regime of Zealandia from convergence to extension with respect to Gondwana remain a matter of debate (Laird and Bradshaw, 2004; Mortimer, 2008; Stowell et al., 2014; Schwartz et al., in press). However, most studies agree that convergent margin magmatism ceased in Zealandia c. 105 Ma and transitioned to extension by c. 90 Ma (Figure 2) (Klepeis et al., 2003; Laird and Bradshaw, 2004; Flowers et al., 2005; Klepeis et al., 2007; Mortimer, 2008; Schwartz et al., in press). Three models have been constructed to explain this transition in tectonics - one model postulates that subduction terminated with the oblique subduction of the Phoenix-Pacific ridge, resulting in capture of Zealandia by the Pacific plate (Laird and Bradshaw, 2004). The second model theorizes that the Phoenix-Pacific ridge ceased activity as it neared the margin of New Zealand once subduction was terminated, this aided in the Pacific plate's capture of New Zealand (Laird and Bradshaw,

2004). Both these models assume a Pacific plate that was moving away from New Zealand, and that New Zealand's attachment to the Pacific plate led to a rapid transition to crustal extension (Laird and Bradshaw, 2004). A third model proposes that the Hikurangi Plateau beneath the Chatham Rise effectively jammed the convergent margin of Gondwana at Zealandia from c. 105 – 100 Ma, which was followed by regional extension (Figure 2; Bradshaw, 1989; Davy et al., 2008; Mortimer, 2008). Rifting of Gondwana caused by extensional tectonics eventually led to the isolation of Zealandia from Gondwana as well as the opening of the Tasman Sea c. 84 Ma (Figure 2) (e.g., Klepeis et al., 2003; Laird and Bradshaw, 2004; Mortimer, 2008).

2.2 Geologic setting of Fiordland magmatic arc

Episodic convergent margin arc magmatism took place in the Median Batholith of Zealandia along the paleo-Gondwana margin from the Carboniferous to the Early Cretaceous, followed by extension, cooling, and exhumation culminating with rifting at 84 Ma and the opening of the Tasman Sea (Klepeis et al., 2003; Flowers et al., 2005). Fiordland comprises a well-exposed, faulted and tilted magmatic arc section from deep (c. 16 kbar) to shallow (c. 8 kbar) crust (Daczko et al., 2002; Klepeis et al., 2004). Previous workers divide Zealandia into two parts - the Western Province (of which the Median Batholith is part) and Eastern Province (Mattinson et al., 1986; Bradshaw, 1989; Mortimer, 2008; Mortimer et al., 2014).

2.2.1 Western Province

The Western Province comprises the rifted fragments of the Triassic to early Cretaceous paleo-Pacific Gondwana margin (Clarke et al., 2000; Hollis et al., 2003). Rocks in the Western Province are the deeper level exposure of the same, shallower rocks

exposed in the west Nelson region of the South Island; these two regions are offset dextrally by c. 480-500 km of movement along the Alpine Fault (Mattinson et al., 1986; Hollis et al., 2004). The lithology of the Western Province includes Late Precambrian gneisses, mid-Paleozoic to Cretaceous metamorphic and plutonic rocks, and early to mid-Paleozoic sedimentary rocks (Mattinson et al., 1986).

The Median Batholith, a part of the Western Province, is the product of episodic subduction-related magmatism from c. 306-105 Ma (Marcotte et al., 2005; Mortimer, 2008; Mortimer et al., 2014). Primarily it comprises subduction-related, I-type plutons as well as volcanic and sedimentary rocks (Clarke et al., 2000; Mortimer, 2008). From c. 306-105 Ma, subduction-related magmatism prevailed and I-type subduction-related magmatism dominated; around 130 Ma, the flux rate of magmatism increased, culminating in the intrusion of the Western Fiordland Orthogneiss from c. 125-115 Ma; magmatism ceased c. 105 Ma with the change in the tectonic regime in Zealandia from convergence to extension (Hollis et al., 2003; Mortimer, 2008).

2.2.2 Eastern Province

The Eastern Province comprises six terranes (Brook Street, Murihiku, Maitai Caples, Waipapa Composite, and Torlesse Composite) which range in age from Permian to Early Cretaceous (Mortimer, 2008). The province itself is bounded by faults, and primarily comprises Cretaceous arc volcanic rocks, sedimentary rocks, and accretionary complexes, which are largely allochthonous in origin (Mattinson et al., 1986; Hollis et al., 2003). Its sedimentary units, particularly its greywacke, likely have an Austrailian or Antarctic detrital source (Mortimer, 2008). Accretion of Eastern Province terranes to the Paleozoic to Cretaceous rocks of the Western Province began in the Permo-Triassic, and

is believed to have ceased by c. 97 Ma as evidenced by alkaline igneous rocks across Zealandia (Clarke et al., 2000; Hollis et al., 2003; Mortimer, 2008).

2.3 Geology of northern Fiordland

Northern Fiordland exposes exhumed lower crustal magmatic arc rocks from paleodepths in a faulted and tilted section between c.8-16 kbar over approximately 50 km from George to Milford Sounds, respectively (Figure 3) (Klepeis et al., 2004). This study focuses on its three primary components – the Arthur River Complex, the Western Fiordland Orthogneiss, and the Median Batholith gneissic basement into which the former intrudes.

2.3.1 Arthur River Complex

The Arthur River Complex outcrops in Milford Sound in northern Fiordland and is the suite into which the WFO intrudes (Figure 3) (Bradshaw, 1990; Clarke et al., 2000; Flowers et al., 2005). To the west it is bordered by the mylonitic Anita Shear Zone; to the east it is bordered by the Darran Complex. Some authors have inferred that the Arthur River Complex represents a metamorphosed and deformed section of the Darran Complex (Figure 3) (Clarke et al., 2000; Hollis et al., 2003). Lithologically, the Arthur River Complex broadly comprises garnet-bearing amphibolitic and leucocratic orthogneisses, as well as minor quartzofeldspathic paragneisses (Bradshaw, 1990; Tulloch et al., 2011).

The Arthur River Complex has been divided into the Milford Gneiss, Harrison Gneiss, Selwyn Creek Gneiss, and Pembroke Granulite (Clarke et al., 2000; Hollis et al., 2003). The Milford Gneiss is a homogenous, garnet- and hornblende-bearing mafic gabbroic gneiss that outcrops in Milford Sound (Clarke et al., 2000; Hollis et al., 2003).

The Harrison and Selwyn Creek Gneisses are largely dioritic banded orthogneisses that also outcrop in Milford Sound (Clarke et al., 2000; Hollis et al., 2003). The Pembroke Granulite comprises amphibolites, trondhjemite veins, dioritic and gabbroic gneisses, and associated garnet granulite reaction zones (Clarke et al., 2000; Klepeis et al., 2003; Hollis et al., 2003; Stowell et al., 2010).

2.3.2 Western Fiordland Orthogneiss

The Cretaceous Western Fiordland Orthogneiss (WFO) is a magmatic arc-derived batholith which represents the last stages of Median Batholith magmatism and intrudes the Arthur River Complex and Paleozoic and Mesozoic country rock (Clarke et al., 2000; Hollis et al., 2003; Hollis et al., 2004; Flowers et al., 2005). The WFO outcrops in western Fiordland between Breaksea Sound to the south and Sutherland Sound to the north and comprises at least seven dioritic and monzodioritic plutons metamorphosed at amphibolite to granulite facies conditions (Figure 1) (Mattinson et al., 1986; Bradshaw, 1990; Hollis et al., 2004; Flowers et al., 2005; Allibone et al., 2009). The emplacement of the WFO from c. 125 – 115 Ma reflects the last pulses of arc magmatism along the convergent paleo-Pacific Gondwana margin and provides insight into the thermal evolution of the long-lived paleo-Pacific Gondwana margin (Hollis et al., 2004).

2.3.3 Paragneiss and orthogneiss basement

Early Paleozoic metasedimentary rocks and orthogneisses of the Median Batholith comprise western Fiordland (Bradshaw, 1990; Clarke et al., 2000; Allibone et al., 2009). One unit in particular is important to differentiate from the other country rock due to its use in this study – the George Sound Paragneiss, first recognized by Bradshaw (1990). It outcrops primarily in George Sound as xenoliths within the intruding WFO, but

has been also observed in Bligh Sound (Figure 3) (Bradshaw, 1990; Hollis et al., 2004). The George Sound Paragneiss ranges in composition from pelitic to semipelitic schists and gneisses, with most rocks bearing garnet (Bradshaw, 1990; Hollis et al., 2004). Previous studies show that its protolith was likely of Permo-Triassic age prior to Cretaceous metamorphic resetting of zircons (Hollis et al., 2004). The intrusion of the WFO during the Cretaceous caused high-temperature metamorphism at c. 630-690°C and pressures c. 9-12 kbar (i.e., amphibolite facies conditions) (Hollis et al., 2004).

2.4 Timing of Cretaceous metamorphism and cooling in northern Fiordland

The metamorphic history of northern Fiordland can be divided into three stages: 1) metamorphism occurring prior to WFO emplacement c. 134 Ma; 2) metamorphism concurrent with the emplacement of the WFO from c. 125 – 115 Ma; and 3) metamorphism and cooling following cessation of WFO magmatism. The Arthur River Complex records Cretaceous metamorphism occurring immediately prior to WFO emplacement (Daczko et al., 2002; Stowell et al. 2010). Tulloch et al. (2011) dates the igneous protolith to the Arthur River Complex at c. 357 Ma, with a granulite-facies metamorphic event occurring c. 134 Ma which partial melted and/or resorbed most of the mid-Paleozoic grains. Stowell et al. (2010) gives U-Pb zircon dates of c. 134 Ma and hypothesize that they were metamorphic in origin. Garnet core Sm-Nd dates of c. 126 Ma at ~850 °C record growth likely due to high-pressure granulite facies metamorphism (Stowell et al., 2010). Daczko et al. (2002) shows elevated temperatures between 750-850 °C occurring in the Arthur River Complex due to partial melting resulting from convergent tectonics. This metamorphic event may have been the precursor to the

magmatic flare-up that emplaced the pluton protoliths of the WFO (Stowell et al., 2010; Tulloch et al., 2011).

High temperature and pressure metamorphic conditions occurred synchronously with the emplacement of the WFO (Clarke et al., 2000; Hollis et al., 2003; Stowell et al., 2010). Zircons from the Arthur River Complex record dates of c. 120 Ma, likely due to contact metamorphism with the WFO (Tulloch et al., 2011). Sm-Nd garnet ages from the Pembroke Granulite as documented by Stowell et al. (2010) indicate that T > 680°C and P = 11-14 kbar occurred between 126.1 ± 2.0 and 122.6 ± 2.0 Ma concurrently with initial pluton emplacement of the WFO. Emplacement of the WFO into the mid to lower crust occurred between c. 125-115 Ma (Mattinson et al., 1986; Hollis et al., 2003; Klepeis et al., 2003; Klepeis et al., 2007; Allibone et al., 2009; Sadorski, 2015). Contemporaneous high-pressure granulite facies metamorphism also occurred during WFO emplacement (Clarke et al., 2000; Daczko et al., 2002; Hollis et al., 2003; Stowell et al., 2010; Tulloch et al., 2011). Contraction following intrusion initiated subsequent tectonic collision-related burial of the WFO in northern Fiordland by c. 20-25 km of continental crust, bringing the batholith to peak high-pressure/high temperature metamorphic conditions (P < 16 kbar, T > 750°C) (Bradshaw, 1990; Clarke et al., 2000; Hollis et al., 2004; Flowers et al., 2005; Allibone et al., 2009).

Events following peak metamorphic conditions in northern Fiordland, including the duration of cooling, remain the most uncertain part of its thermochronologic history. Flowers et al. (2005) speculate the cooling history of northern Fiordland parallels that of central Fiordland. Initial rapid cooling occurred in central Fiordland after WFO intrusion into the mid-crust which caused peak metamorphic conditions (16 kbar and T > 750°C)

during burial by c. 25 km of continental crust by c. 116 Ma (Bradshaw, 1990; Klepeis et al., 2004; Flowers et al., 2005). However, recent studies have scrutinized the high-pressure/loading story expounded by earlier literature (e.g., Bradshaw, 1990; Klepeis et al., 2004; Flowers et al., 2005). Garnet P-T-t data for the Malaspina pluton in central Fiordland shows that garnet grew without significant pressure changes during granulite-facies metamorphism; at most, high Ca rims on garnets suggest pressure changes of ≤ 1.5 kbar (Stowell et al., 2014). These data suggest that pressure change and exhumation were not responsible for keeping the lower crust at garnet-growth conditions; instead, Stowell et al. (2014) hypothesizes that the Gondwana crust was >40 km thick during WFO emplacement, sustaining garnet granulite metamorphic conditions during the arc transition from convergence to extension. Daczko and Halpin (2009) affirms that because of the stability of a garnet granulite mineral assemblage from northern Fiordland, it is plausible for such an assemblage to form with <5 km of crustal loading.

Isobaric cooling of the magmatic arc, as elucidated by $^{206}Pb/^{238}U$ titanite thermochronology, occurred from 113.4-111.1 Ma through 650-600°C (Flowers et al., 2005). Sm-Nd garnet from Stowell et al. (2014) show that the lower crust at c. 112 Ma was 800-900 °C, in contrast to a $^{206}Pb/^{238}U$ titanite date from Flowers et al. (2005) that indicates the lower crust was cool at ~650 °C at c. 112 Ma. Other studies similarly suggest that northern Fiordland was rheologically strong, dry (due to dehydration at granulite facies conditions), and cool (T > 700°C) by c. 116 Ma (Klepeis et al., 2004). Rutile $^{206}Pb/^{238}U$ thermochronology shows that cooling through 450-400°C did not occur in central Fiordland until c. 70 Ma, suggesting a protracted cooling history of 40-45 Ma (Flowers et al., 2005).

Previous studies conducted in northern Fiordland exhibit contradictory cooling histories. Studies specifically of the Arthur River Complex indicate that rapid cooling occurred between c. 120-90 Ma – one titanite date from Milford Sound implies rapid cooling to 600-650 °C by c. 120 Ma (Flowers et al., 2005). Milford and Harrison Orthogneiss K-Ar hornblende and plagioclase dates suggest cooling of the Arthur River Complex by c. 110-90 Ma (Gibson et al., 1988; Nathan et al., 2000; Daczko et al., 2002; Hollis et al., 2003). Apatite dates from Mattinson et al. (1986) indicate that cessation of metamorphism along with exhumation of mid and lower crust occurred by c. 90 Ma at temperatures less than 300-400°C, which agree with the aforementioned K-Ar hornblende dates. However, one apatite date from the Darran Complex, which lies east and partly in fault contact with the Arthur River Complex, records c. 128 Ma cooling to 400-450 °C, implying that no reheating occurred as a result of WFO emplacement (Flowers et al., 2005). In contrast, Sm-Nd garnet ages < 110 Ma (c. 109, garnet rim and c. 94 Ma, garnet reaction zone) from the Pembroke Granulite (also in the Arthur River Complex) indicate late garnet growth due to partial melting and slow cooling, and garnet dates c. 94 Ma show that the lower crust remained hot (~850 °C) for 20-30 Ma prior to exhumation and further cooling (Stowell et al., 2010). Further, Stowell et al. (2014) found via Sm-Nd garnet dates that garnet granulite metamorphism in central Fiordland occurred >10 Ma after garnet granulite facies metamorphism in northern Fiordland. Clearly, further thermochronologic work is necessary to elucidate the complex metamorphic and cooling history of northern Fiordland.

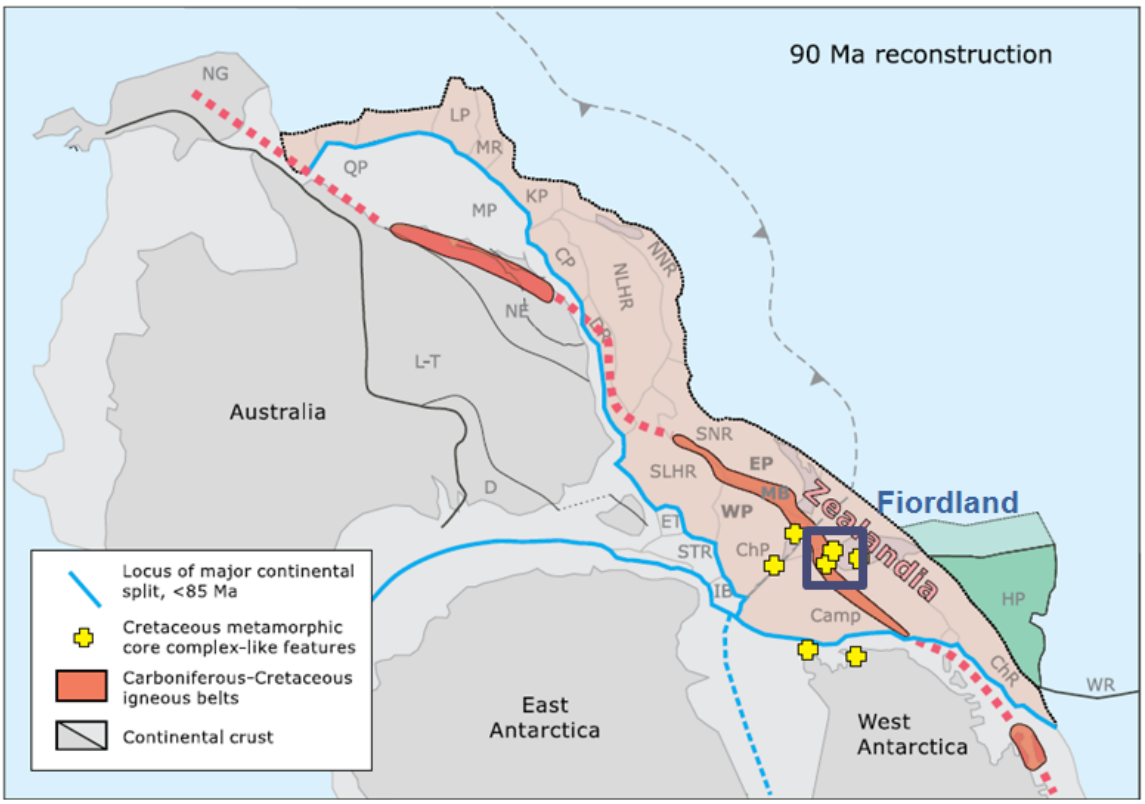

Figure 2: 90 Ma reconstruction showing of components of the supercontinent Gondwana prior to breakup. Red indicates location of convergent margin magmatism-related plutons; light blue lines indicate location of future rifts that will open up the Southern Ocean and Tasman Sea. Dark blue box indicates location of Fiordland (modified from Mortimer, 2008). NG=New Guinea, QP=Queensland Plateau, MP=Marion Plateau, LP=Louisiade Plateau, MR=Mellish Rise, KP=Kenn Plateau, CP=Chesterfield Plateau, DR=Dampier Ridge, NLHR, SLHR=Northern and Southern Lord Howe Rise, NNR, SNR=Northern and Southern Norfolk Ridge, ET=East Tasman Rise, STR=South Tasman Rise, ChP=Challenger Plateau, Camp=Campbell Plateau, ChR=Chatham Rise, HP=Hikurangi Plateau (pale green part now subducted beneath Kermadec Trench), WR=Wishbone Ridge, IB=Iselin Bank. Geological features: D=Delamerian Orogen, L-T=Lachlan-Thomson Orogen, NE=New England Orogen, EP=Eastern Province, WP=Western Province, MB=Median Batholith.

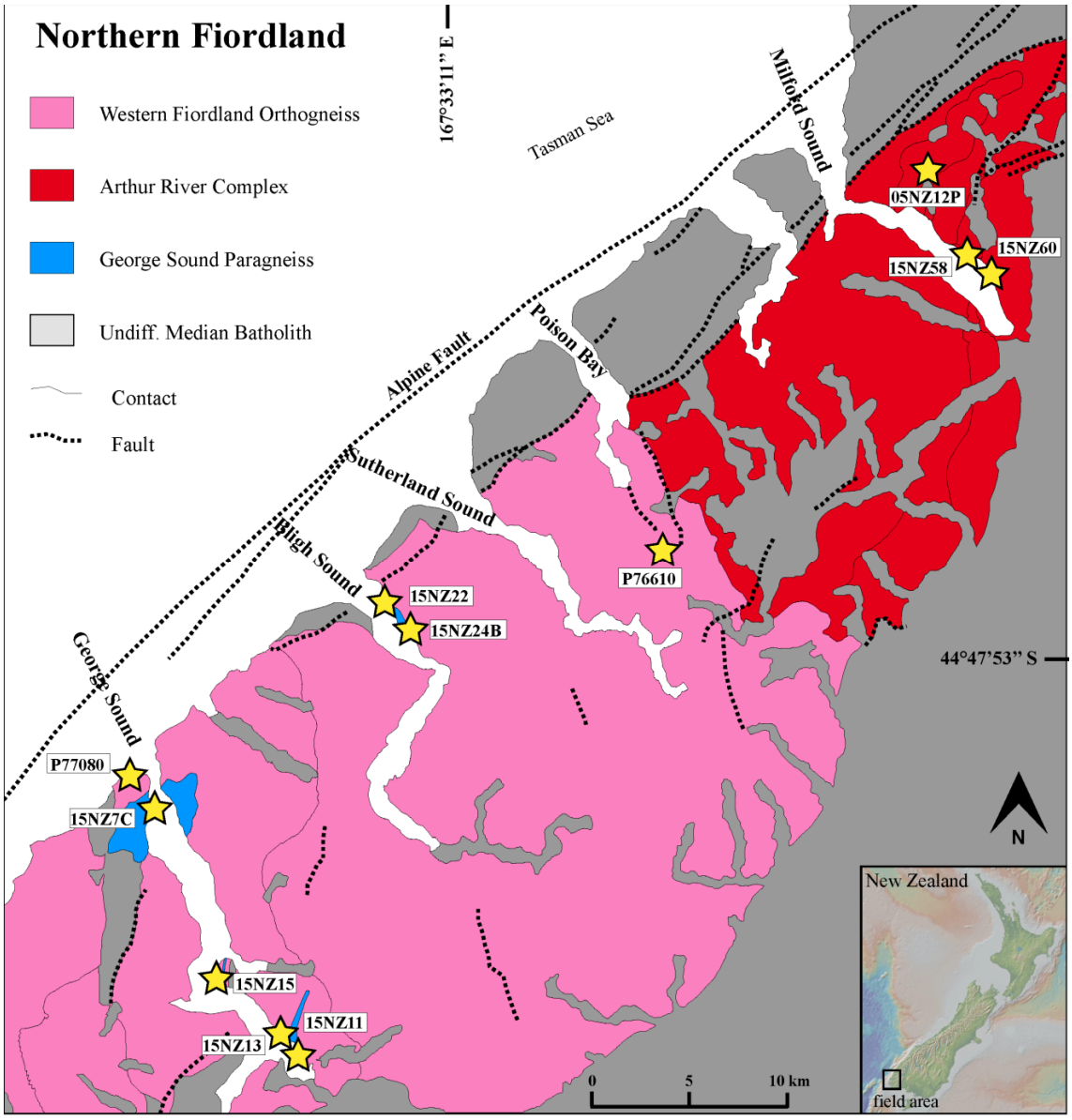

Figure 3: Simplified geologic map of northern Fiordland, New Zealand. Yellow stars indicate sample locations for this study.

3. METHODS

3.1 Sampling

Samples for this study were primarily collected during the January 2015 field season in Fiordland National Park, South Island, New Zealand (samples beginning "15NZ-") between George Sound to the south and Milford Sound to the north (Figure 3). These were supplemented by samples from the GNS archive collected by various workers (samples beginning with "P-").

In order to illuminate the cooling history for the deepest (Milford Sound) to shallowest (George Sound) areas of the exposed arc, representative samples were chosen from north to south in an arc-parallel transect, as well as from west to east (Figure 3) (Klepeis et al., 2003). An ultraviolet light was utilized to preliminarily assess zircon abundance in samples; observations of thin sections via optical microscopy informed the selections for titanite-bearing samples. Eleven total samples were selected and include 9 zircon-bearing and 5 titanite-bearing samples. Some samples contain both phases.

3.2 Mineral separation and sample preparation

Zircon and titanite were obtained from each sample via standard mineral separation techniques, carried out at California State University, Northridge (CSUN). Whole rock samples were crushed into sand-sized particles and separated by density via Wilfley water table. Heaviest separates were sieved and the < 250 μm fraction processed through a Frantz isodynamic separator at 0.1, 0.5, 1.0, and 1.5 A. The remaining nonmagnetic fraction was taken through methyl iodide (MI) for the purposes of density separation to isolate zircon.

Individual grains of both phases were picked for analysis under a binocular microscope. Clear, colorless, inclusion-free grains were targeted for analysis.

Metamorphic zircons – characterized by their rounded, anhedral shapes – were picked to constrain the age of metamorphism throughout the northern arc (Corfu et al., 2003). Approximately 60-100 grains per sample were mounted on a 25 mm diameter by 4 mm thick epoxy disc and ground and polished to a 0.25 micron finish to expose interiors. In order to avoid inclusions, cracks, and imperfections in the grains during analysis, zircons were imaged via cathodoluminescence (CL) with a Gatan MiniCL detector on a FEI Quanta 600 variable pressure environmental scanning electron microscope (SEM) at CSUN; titanites were imaged with a backscatter electron (BSE) detector on the SEM at CSUN.

Thin sections for in-situ titanite LASS analysis were polished with 0.25 micron colloidal silica and high-resolution scans, and BSE maps via SEM were taken prior to analysis to facilitate locating titanites.

3.3 U-Pb zircon geochronology

Metamorphic $^{206}Pb/^{238}U$ zircon dates were determined by Sensitive High Resolution Mass Spectrometer Reverse Geometry (SHRIMP-RG) at Stanford University, co-operated by the U.S. Geological Survey. Dates were collected during two analytical sessions: from 03/03/2015-03/04/2015 and from 10/15/2015-10/16/2015. Prior to analysis, the epoxy mounts were washed with a 1N HCl solution and thoroughly rinsed in distilled water, dried in a vacuum oven, and coated with gold. The mounts were stored at high pressure (10-7 torr) for several hours before being moved into the source chamber of the SHRIMP-RG to minimize degassing of the epoxy and isobaric hydride interferences and masses 204-208.

Secondary ions are sputtered from the target spot using an O_2- primary ion beam, which was accelerated at 10 kV and had an intensity varying from 3.2 to 3.6 nA during the first session and 3.8 to 4.6 nA during the second. The primary ion beam spot had an ellipse-shape approximately 18 x 25 microns and a depth of ~2.0 micron for the analyses performed in this study. Before every analysis, the sample surface was cleaned by rastering the primary beam for 60 seconds, and the primary and secondary beams were auto-tuned to maximize transmission. The duration of procedure typically required 2.5 minutes prior to data collection. The acquisition routine included analysis of $^{30}Si^{16}O^+$, $^{48}Ti^+$, $^{49}Ti^+$, $^{56}Fe^+$, $^{89}Y^+$, 9-REE ($^{139}La^+$, $^{140}Ce^+$, $^{146}Nd^+$, $^{147}Sm^+$, $^{153}Eu^+$, $^{155}Gd^+$, $^{162}Dy^{16}O^+$, $^{166}Er^{16}O^+$, $^{172}Yb^{16}O^+$), a high mass normalizing species ($^{90}Zr_2{}^{16}O+$), followed by $^{180}Hf^{16}O^+$, $^{204}Pb^+$, a background measured at 0.045 mass units above the $^{204}Pb^+$ peak, $^{206}Pb^+$, $^{207}Pb^+$, $^{208}Pb^+$, $^{232}Th^+$, $^{238}U^+$, $^{232}Th^{16}O^+$, and $^{238}U^{16}O^+$. Trace element measurements (Ti, Fe, Y, Hf, REE) were measured briefly (typically 1 to 5 sec/mass) immediately before the geochronology peaks, and in mass order. For the first session, $^{232}Th^+$ was not measured. All peaks were measured on a single EPT® discrete-dynode electron multiplier operated in pulse counting mode with 5 scans (peak-hopping cycles from mass 46 through 254). The counting times on each peak were varied according to the sample age and the U and Th concentrations to improve counting statistics and age precision. Measurements were made at mass resolutions of $M/\Delta M$ = 8200-8800 (10% peak height), which eliminates interfering molecular species, particularly for the REE.

For mounts 15CSUN57 and 15CSUN66, zircon concentration data for U, Th and all measured trace elements were calculated relative to MADDER (3435 ppm U; Barth and Wooden, 2010), which was co-mounted with unknowns on each mount. Calculated

model ages for zircon were standardized relative to Temora-2 (416.8 Ma; Black et al., 2004), which were analyzed repeatedly throughout the duration of the analytical session. Data reduction for geochronology followed the methods described by Williams (1997), and Ireland and Williams (2003), and used the MS Excel add-in programs Squid2.51 and Isoplot3.764 of Ken Ludwig (2009; 2012). The measured $^{206}Pb/^{238}U$ was corrected for common Pb using ^{207}Pb, whereas $^{207}Pb/^{206}Pb$ was corrected using ^{204}Pb. The common-Pb correction was based on a model Pb composition from Stacey and Kramers (1975). All reported $^{206}Pb/^{238}U$ and $^{207}Pb/^{206}Pb$ model ages and uncertainties (2σ) include error summed in quadrature from the external reproducibility of the standard Temora-2 during an individual analytical session (~24 hours).

Data reduction for the trace element concentrations were performed in MS Excel. Average count rates of each element of interest were ratioed to $^{30}Si^{16}O$ to account for any primary current drift, and the derived ratios for the unknowns were compared to an average of those for the standards to determine concentrations. Spot to spot precisions (as measured on the standards) varied according to elemental ionization efficiency and concentration. For the MADDER zircon, precisions generally ranged from about ±3% for Hf, ±5-10% for the Ti, Fe, Y and HREE, ±10-15%, and up to ±40% for La which is present most often at the ppb level (all values at 2σ).

3.4 U-Pb titanite geochronology

Titanite dates were collected via the Laser Ablation Split-Stream Inductively Coupled Plasma Mass Spectrometer (LASS-ICP-MS) at the University of California, Santa Barbara (UCSB) during one session from 06/25/2015 to 06/26/2015. Methods closely follow those outlined in Kylander-Clark et al. (2013) and Spencer et al. (2013).

Samples were ablated in grain mounts using a Photon Machines 193 nm ArF excimer ultraviolet laser with a HelEx ablation cell coupled to a Nu Instruments Plasma high-resolution multi-collector inductively coupled plasma mass spectrometer (MC-ICP-MS). Laser spot diameter was ~40 μm for titanite and 30 μm for NIST 610. The laser was fired twice with a spot size of 53 μm to remove common Pb from the sample surface and this material was allowed to wash out for 15 seconds. Titanites were then ablated at 4 Hz for 20 seconds, resulting in a pit depth of ~8 μm. Masses ^{204}Pb+Hg, ^{206}Pb, ^{207}Pb, and ^{208}Pb were measured on ion counters, and masses ^{232}Th and ^{238}U were measured on Faraday detectors. Analyses of unknowns were bracketed by analyses of primary reference material USGS-BLR provided by J. Aleinikoff to the USGS-Stanford SHRIMP-RG laboratory (Aleinikoff et al., 2007). A second titanite reference material, UCSB-BLR, was collected from the same location as USGS-BLR and was used as a secondary standard. Several other in-house standards were analyzed to monitor reproducibility. These include: BHVO and SJ41 (389 Ma).

Titanite LASS data were reduced using the Iolite (v. 2.5) plug-in (Paton et al., 2011) for the Wavemetrics Igor Pro software program. Baselines intensity measurements were performed prior to each analysis, and the mean and standard error of the measured backgrounds and peaks were calculated after rejection of outliers more than 2 standard errors beyond the mean. Uncertainty of individual ^{206}Pb/^{238}U measurements is dominated by counting statistics and signal stability. The typical uncertainty can be represented by the Tukey's biweight mean of ~1.9% calculated for the long-term measurement of >3400 unknowns (Spencer et al., 2013). Individual ^{207}Pb/^{206}Pb measurements are much more precise yielding a long-term, Tukey's biweight mean of 0.2%. An additional 2% external

error is added in quadrature to $^{207}Pb/^{206}Pb$ measurements to account for variation in ablation or transport characteristics.

Isotopic ratios for each analysis were plotted on Tera-Wasserburg (1972) diagrams using Isoplot (Ludwig, 2012). Analyses commonly have sufficient spread in $^{238}U/^{206}Pb$ and $^{207}Pb/^{206}Pb$ to define an isochron without the need to assume a common $^{207}Pb/^{206}Pb$ value from a model (e.g., Stacey and Kramers, 1975) or from a low-U mineral presumed to be in equilibrium with titanite. For samples with small spread in U-Pb ratios (and thus a poorly constrained common $^{207}Pb/^{206}Pb$ value) we anchored the ratio to the Stacey and Kramers (1975) value of 0.84 ± 0.01, appropriate for differentiation ages of ca. 120-100 Ma. In most cases, dates with low spread in $^{238}U/^{206}Pb$ and $^{207}Pb/^{206}Pb$ have high radiogenic-Pb/common-Pb values such that uncertainties in initial common $^{207}Pb/^{206}Pb$ have little effect on reported dates. All dates are reported at 95% confidence interval and are assigned 2% combined systematic and analytical uncertainties, which correspond to total errors of ~2.0-2.5 Ma.

3.5 Statistical parameters for zircon and titanite

Statistical treatment of titanite and zircon dates involves calculation of MSWD, or mean square weighted deviation, to distinguish between accepted analytical data and observed analytical data. MSWD is defined as:

$$\text{MSWD} = f^{-1} \Sigma(\Delta y_i^2 / \sigma_i^2)$$

Whereby $f = (n-1)$ degrees of freedom, and n represents the total number of data points, $\Delta y_i = y_i - ax_i - b$, is the deviation of the ith point and $\sigma_i^2 = \sigma^2 (\Delta y) = a^2\sigma_{xi}^2 + \sigma_{yi}^2$, is the square of the error. An MSWD value close to or equal to 1 occurs if the assigned error is accurately described by the data. When the MSWD is >> 1, the scatter of data is beyond

analytical uncertainties due to either: 1) non-analytical errors, such as a geologic phenomenon that creates the deviation from the mean, or 2) an underestimation of the assigned error. MSWD values << 1 indicate that the scatter of data is much less than the assigned analytical uncertainty and can result from overestimation of the analytical error or unrecognized error correlations.

3.6 Titanium-in-zircon thermometry

Zircon metamorphic temperatures were calculated using the MS Excel add-in program Squid2.51 via the SHRIMP-RG at Stanford University. Measured values of ^{48}Ti ppm in each sample were used and $a_{Ti02} = 1$ based on the presence of rutile or ilmenite in analyzed samples (Hayden et al., 2008). An average temperature value was calculated using n = number of analyses per sample. All temperature error values were calculated at 2σ based on the standard deviation of each calculated temperature.

3.7 Zirconium-in-titanite thermometry

Zirconium concentrations in titanite were obtained by LASS-ICP-MS at UCSB. Methods from Hayden et al. (2008) were used to calculate titanite temperatures. Temperature uncertainties of 5-10°C result from analytical uncertainties of Zr measurements, which range from 5-10% (2σ). Specifically, the following equation was used from Hayden et al. (2008):

$$T\ (°C) = [7708+960(P)]/[10.52-\log(a_{TiO2})-\log(a_{SiO2})-\log(\text{ppm Zr, titanite})]-273$$

Activities of TiO_2 and SiO_2 were assumed to equal 1, due to the presence of rutile in most samples and the presence of zircon in all samples (i.e., Hayden et al., 2008). Pressures, P, were estimated from data shown in Klepeis et al. (2007). All titanite samples except P76610, for which 1.3 GPa was used, assumed a pressure of 0.9 GPa (Klepeis et al.,

2007). Peak pressure estimates throughout Fiordland for granulite to amphibolite facies metamorphism range from 0.7-1.6 GPa (Bradshaw, 1989; Klepeis et al., 2003; Klepeis et al., 2007). Given this range and that a 0.4 GPa uncertainty results in a ~50°C calculated temperature uncertainty, we apply a ± 50°C uncertainty to all estimated titanite temperatures.

4. RESULTS

4.1 Petrography

Petrographic analysis was carried out for all samples via petrographic microscope. Photomicrographs were taken of each sample in order to document the mineral phases present as well as relevant textures and/or deformation features (Figure 4). Modal abundances of phases were obtained based on visual estimates. A summary of petrographic observations, as well as sample locations and descriptions, may be found in Table 1.

4.1.1 George Sound Paragneiss - 15NZ7C

Sample 15NZ7C is located at the mouth of George Sound, and comes from an outcrop of George Sound Paragneiss (Figure 3; Table 1). It is medium grained, largely felsic, and has moderate foliation (Figure 4a). Felsic grains are sub to anhedral; mafic grains are largely subhedral. Some quartz grains show undulose extinction and subgrains. Some biotite grains show kinking. Garnet porphyroclasts have an average diameter of 0.5-1 mm, are largely fractured, and display sub to anhedral crystal habits (Figure 4a).

4.1.2 George Sound Paragneiss - 15NZ11

This sample is the furthest eastern sample from George Sound, and is from the George Sound Paragneiss (Figure 3; Table 1). It has a bimodal grain size distribution between coarse and fine, and is weakly to moderately foliated (Figure 4b). Quartz grains are anhedral and display undulose extinction. Albite twins are present in plagioclase grains. Biotite and sillimanite are frequently the smallest phases present. Garnet porphyroclasts have grain diameters averaging 1-1.5 mm and are sub to euhedral and commonly fractured (Figure 4b).

4.1.3 George Sound Paragneiss - 15NZ13

15NZ13 is from the George Sound Paragneiss and was collected in George Sound (Figure 3; Table 1). The sample is fine grained (average grain diameter ~0.5 mm), felsic, and weakly foliated (Figure 4c). Felsic phases are anheral in crystal habit. Quartz grains display undulose extinction. Plagioclase grains have albite twins. K-feldspar grains display tartan twinning. Mafic phases are largely subhedral in crystal habit. Subhedral, trace amounts of garnet are present with diameters less than 50 μm (Figure 4c).

4.1.4 George Sound Paragneiss - 15NZ15

This sample is from the George Sound Paragneiss, collected from the north wall of George Sound (Figure 3; Table 1). 15NZ15 is fine to medium grained, dominantly felsic, moderately foliated and compositionally banded (Figure 4d). Quartz grains are anhedral and show undulose extinction. Garnet porphyroblasts are sub to euhedral (diameters averaging 0.5-1 mm), heavily fractured, and show resorption texture. Plagioclase grains are sub to anhedral and show albite twinning. Hornblende grains are subhedral and show resorption texture (Figure 4d). Zircon, rutile, and titanite are present in trace amounts.

4.1.5 George Sound Paragneiss - 15NZ22

15NZ22 is from the George Sound Paragneiss, sampled from the northern shore at the mouth of Bligh Sound (Figure 3; Table 1). Foliation is weak to moderate, with felsic phases dominating the mineral assemblage (Figure 4e). Quartz grains are anhedral and fine (~200 μm in diameter) with some grains showing undulose extinction. Plagioclase grains display albite twinning and some deformation twins, and are also andedral and fine-grained (~200 μm). K-feldspar grains are fine and anhedral and display tartan

twinning and some deformation twinning. Biotite and hornblende grains are sub to anhedral. Titanite grains are sub to euhedral and average 100 μm in diameter (Figure 4e).

4.1.6 George Sound Paragneiss - 15NZ24B

This sample is located just east of sample 15NZ22 in Bligh Sound, and is also from the George Sound Paragneiss (Figure 3; Table 1). 15NZ24B is fine-grained, quartzofeldspathic, and compositionally banded, showing moderate foliation (Figure 4f). Quartz grains are anhedral, with some grains showing subgrains and undulose extinction. Plagioclase grains are largely anhedral and display albite twining; additionally, some grains show deformation twins. Pyroxenes and hornblende grains are sub to anhedral and show resorption texture. Titanite grains are large (average diameter ~200 μm) and are sub to euhedral in crystal habit (Figure 4f).

4.1.7 Harrison Gneiss - 15NZ58

This sample is from the Harrison Gneiss, which is part of the Arthur River Complex, and was taken from the northern side of Milford Sound (Figure 3; Table 1). This sample shows moderate to heavy foliation defined by compositional banding and coarse grains (Figure 4g). Hornblende is subhedral and shows resorption texture. Quartz shows subgrains and undulose extinction; grains are sub to anhedral. Plagioclase is sub to anhedral and shows albite twinning and deformation twins in some grains. Clinozoisite is fibrous in form and subhedral. Garnet porphyroblasts are sub to euhedral, fractured, and shows resorption texture with an average diameter of 1 mm (Figure 4g).

4.1.8 Selwyn Creek Gneiss - 15NZ60

Sample 15NZ60 is from the Selwyn Creek Gneiss, which is a member of the Arthur River Complex. The sample was taken from the northern wall of Milford Sound

(Figure 3; Table 1). As observed by previous authors, this sample is a dioritic banded orthogneiss, medium to coarse-grained (Hollis et al., 2003). Quartz and plagioclase grains are sub to anhedral, with quartz grains displaying undulose extinction and subgrain development (Figure 4h). Plagioclase grains display albite twinning and Carlsbad twinning; deformation twins were also observed. Hornblende is subhedral and is the primary mafic mineral forming mafic bands. Kyanite is subhedral and elongate, usually present next to hornblende grains. Biotite is also present as a minor phase and is subhedral in crystal habit (Figure 4h).

4.1.9 Pembroke Granulite - 05NZ12P

Sample 05NZ12P was collected by Stowell from the Pembroke Granulite (a member of the Arthur River Complex) in Pembroke Valley on the northern side of Milford Sound (Figure 3; Table 1). The rock is a dioritic gneiss, which contains a garnet reaction zone and leucosome (Stowell et al., 2010). Its mineral assemblage is predominantly hornblende, clinopyroxene, and plagioclase; minor amounts of biotite and elongate clinozoisite crystals, as well as trace amounts of zircon, garnet, and rutile, are also present (Stowell et al., 2010).

4.1.10 Worsley Pluton - P76610

This sample comes from the Worsley Pluton as exposed northeast of Sutherland Sound (Figure 3; Table 1). P76610 exhibits moderate foliation and is medium to coarse-grained (Figure 4i). Quartz is subhedral to anhedral, with some grains exhibiting undulose extinction and subgrains. Biotite grains are subhedral, fine to coarse-grained, and show minor chloritization. Plagioclase grains are largely subhedral, with some grains showing albite twinning, deformation twins, and kinked twins. Kyanite is sub to euhedral

and often shows resorption texture. Garnet porphyroclasts are present (diameter average = 1.5 mm) and are moderately to heavily fractured. Clinozoisite is present as a minor phase, often appearing kinked and fibrous in crystal habit. Titanite grains are sub to euhedral, with the largest grains averaging 250 μm in diameter (Figure 4i).

4.1.11 McKerr Intrusives - P77080

This sample was taken from the McKerr Intrusives that outcrop south of George Sound (Figure 3; Table 1). P77080 has moderate gneissic foliation, and fine to medium-grained phases (Figure 4j). Quartz is sub to anhedral, with some grains displaying undulose extinction and subgrain development. Plagioclase is sub to anhedral, with some grains showing albite twins and/or deformation twins. Hornblende is fine to coarse grained (50-500 μm in diameter), subhedral, and the primary mafic phase. Biotite is fine to medium grained (~100-200 μm in diameter), sub to euhedral and elongate. Minor clinozoisite is present, and fibrous in crystal habit (diameter ~50 μm). Small, euhedral garnet is present throughout sample (~50 μm diameter). Titanites are subhedral, with an average diameter of about 200 μm. Rutile is also present in trace amounts (Figure 4j).

4.2 U-Pb zircon geochronology

Between 60 and 100 zircons were picked and mounted per sample, depending on abundance from mineral separates. Rims were targeted for SHRIMP-RG analysis in order to obtain dates of metamorphism for all samples. All reported $^{238}U/^{206}Pb$ dates are weighted averages with 2σ errors.

4.2.1 George Sound (15NZ7C, 15NZ11, 15NZ13, 15NZ15)

Zircons from sample 15NZ7C have average diameter between 50 and 100 μm (Figure 5a). Of the ten spots targeted for analysis, only two yielded concordant dates with

a $^{206}Pb/^{238}U$ date of 120.0 ± 26 (MSWD = 2.2) (Figure 6a; Table 2). This date was chosen as the probable metamorphic date for this sample as it a) agrees with other metamorphic zircon ages from George Sound (15NZ11) and b) agrees with an age for young zircons obtained via LA-ICP-MS (121.3 ± 2.3 Ma, n = 12, MSWD = 0.36; Quezada and Schwartz, unpubl. data). Uranium concentrations were high, with values of 278 and 1310 ppm. Thorium concentrations were comparatively low, with values of 10 and 12 ppm. Values for Th/U range between 0.010 and 0.359 (Table 3).

Sample 15NZ11 has zircons with diameters averaging 100 μm, frequently with thick metamorphic rims (Figure 5b). Nine spots were analyzed, four of which were concordant, giving a $^{206}Pb/^{238}U$ date of 121.3 ± 1.6 Ma (MSWD = 0.93) (Figure 6b; Table 2). Uranium concentrations range from approximately 560 to 1400 ppm; thorium concentrations range from 7 to 12 ppm. Additionally, Th/U range between 0.007 and 0.28 (Table 3).

The average diameter of zircons in sample 15NZ13 is 200 μm, with their morphology being more angular than zircons in sample 15NZ11 (Figure 5c). Data were also more homogeneous than 15NZ11, with eight out of nine spots yielding a concordant $^{206}Pb/^{238}U$ date of 116.0 ± 2.3 Ma (MSWD = 0.54) (Figure 6c; Table 2). Concentrations of uranium range between 153 and 636 ppm, while concentrations of thorium range from 53 and 191 ppm. Th/U concentrations range from 0.116 to 0.49 (Table 3).

Zircons from sample 15NZ15 are large (200 to 250 μm in diameter) and generally more euhedral than those in 15NZ11 and 15NZ13 (Figure 5d). All six spots gave concordant dates, with a $^{206}Pb/^{238}U$ date of 116.4 ± 4.8 Ma (MSWD = 3.2) (Figure 6d;

Table 2). Uranium concentrations fall between 69 and 251 ppm; thorium concentrations range between 34 and 96 ppm (Table 3).

4.2.2 Bligh Sound (15NZ22, 15NZ24B)

Sample 15NZ22 has zircons with an average diameter of 250 μm with some grains showing oscillatory zoned cores (Figure 5e). All six analyses are concordant, with a $^{206}Pb/^{238}U$ date of 119.9 ± 1.8 Ma (MSWD = 1.3) (Figure 6e; Table 2). Both uranium and thorium concentrations show moderate variability, with uranium concentrations ranging between 183 and 845 ppm, and thorium concentrations ranging between 52 and 688 ppm. Th/U ratios range between 0.295 and 0.841 (Table 3).

Zircon from 15NZ24B are patchy and largely anhedral, with an average diameter of approximately 250 μm (Figure 5f). Nine spots were analyzed, with five yielding concordant data, and a $^{206}Pb/^{238}U$ date of 120.1 ± 2.4 Ma (MSWD = 0.41) (Figure 6f; Table 2). Uranium concentrations are variable, ranging between 141 and 722 ppm. Thorium concentrations range between 50 and 252 ppm. Values for Th/U range between 0.106 and 0.488 (Table 3).

4.2.3 Milford Sound (15NZ58, 15NZ60, 05NZ12P)

Sample 15NZ58 zircons are largely anhedral and have sparse metamorphic rims (Figure 5g). Nine total analyses were carried out, and two distinct age populations were identified. The older population yielded a $^{206}Pb/^{238}U$ date of 146.5 ± 1.4 Ma (n = 5, MSWD = 0.63; Decker et al., unpub.). Three spots comprise the younger data set, yielding a $^{206}Pb/^{238}U$ date of 131.3 ± 7.7 Ma (MSWD = 4) (Figure 6g; Table 2). An older population was also identified by targeting cores on LASS-ICP-MS, with an age agreeing with the older SHRIMP $^{206}Pb/^{238}U$ date of 146.2 ± 1.2 Ma (Decker et al., unpub.). We

interpret that the older dates likely date crystallization, while the younger date may date metamorphism in the Harrison Gneiss. Uranium concentrations are high, ranging from 608 to 1783 ppm. Thorium concentrations are similarly elevated but span a wider range, from 119 to 836 ppm. Th/U ratios for the older population range between 0.50 and 108; Th/U ratios for the younger population range between 0.07 and 1.16 (Table 3).

Zircons from sample 15NZ60 have an average diameter of 200 μm and feature thick rims (> 30 μm) (Figure 5h). Four analyses yielded an older age population (143.9 ± 2.0, MSWD = 0.2, n = 4), and three analyses yielded a younger age population. These three younger analysis give a $^{206}Pb/^{238}U$ date of 134.9 ± 3.1 Ma (MSWD = 0.84) (Figure 6h; Table 2). Two analyses of cores for this sample show considerably older dates; LASS analysis records a $^{206}Pb/^{238}U$ date of 176.9 ± 3.3 Ma, and SHRIMP analysis records a $^{206}Pb/^{238}U$ date of 179.6 ± 5.2 Ma (Decker et al., unpub.). We interpret the older Selwyn Creek Gneiss date to reflect the age of crystallization, and the younger to reflect the date of metamorphism. Uranium concentrations are moderate and fall between 126 and 284 ppm; thorium concentrations range between 34 and 170 ppm. Values for Th/U range between 0.17 and 0.65 (Table 3).

The average diameter of zircon from sample 05NZ12P is ~250 μm (Figure 5i). Five out of seven analyses yielded concordant results, with a $^{206}Pb/^{238}U$ date of 126.5 ± 2.7 Ma (MSWD = 0.88) (Figure 6i; Table 2). Uranium concentrations range between 97 and 463 ppm; thorium concentrations range between 70 and 443 ppm. Values for Th/U fall between 0.549 and 0.99 (Table 3). Stowell et al. (2010) reported LA-MC-ICPMS dates of 134.2 ± 2.9 Ma and 127.2 ± 2.5 Ma for this same sample. For these as well as other zircon analyses from the Pembroke Granulite, Stowell et al. (2010) interprets these

dates to constrain high-pressure metamorphism occurring between 129.4 and 120.6 Ma, making them indistinguishable from Sm-Nd garnet dates and thus also recording metamorphism and partial melting. Additionally, Stowell et al. (2010) reports a garnet Sm-Nd date of 108.9 ± 5.6 Ma from this sample.

4.3 U-Pb titanite geochronology

Depending on abundance, between 40 and 80 titanite grains were picked and mounted per sample. Up to 40-50 spots per sample were picked during LASS-ICP-MS analysis. On large grains, traverses of grains (e.g., Figure 7a) where 2 to 13 spots per grain were analyzed were done in order to elucidate the complicated (re)crystallization history of our titanites (see Discussion section). All titanite analyses plotted along Discordia arrays. We interpret the lower intercept of these discordant arrays as the date of metamorphism and/or (re)crystallization of titanite. All reported $^{206}Pb/^{238}U$ data are lower intercept ages, with 2σ error.

4.3.1 George Sound (P77080, 15NZ15)

Titanite from sample P77080 have an average diameter between 150 and 200 μm, and frequently feature cracks and inclusions which were avoided during analysis (Figure 8a). From 40 analyses, 38 plot along a discordant array, with a lower intercept $^{206}Pb/^{238}U$ date of 112.0 ± 2.4 Ma (MSWD = 0.56) (Figure 9a; Table 4). Both uranium and thorium concentrations are low for this sample, as well as for all analyzed titanite samples. Uranium concentrations average 13 ppm, while thorium concentrations average 11.6 ppm (Table 5).

The average diameter for titanites from sample 15NZ15 is approximately 100 μm (Figure 8b). Seventeen analyses from this sample form a discordant array, with a lower

intercept $^{206}Pb/^{238}U$ date of 94.0 ± 2.3 Ma (MSWD = 2.1) (Figure 9b; Table 4). The mean uranium concentration is 24 ppm, while the mean thorium concentration is 60 ppm (Table 5).

4.3.2 Bligh and Sutherland Sounds (15NZ22, 15NZ24B, P76610)

Sample 15NZ22 titanites have an average diameter of 200 to 250 μm, and frequently contain inclusions and fractures (Figure 8c). Twenty-four analyses yield a $^{206}Pb/^{238}U$ date of 103 ± 21 Ma (MSWD = 0.043) (Figure 9c; Table 4). The large error for this sample can be partially explained by the extremely low average uranium and thorium concentrations of 2.84 and 0.58 ppm, respectively (Table 5).

Titanites from sample 15NZ24B display bimodal grain sizes, with some grains averaging 100 μm in diameter and other averaging 250 μm in diameter (Figure 8d). A total of 44 analyses formed a discordant array, yielding a lower intercept $^{206}Pb/^{238}U$ date of 104.8 ± 1.6 Ma (MSWD = 3.4) (Figure 9d; Table 4). This sample has the highest average uranium and thorium concentrations of analyzed titanites; uranium concentrations average 117 ppm, while thorium concentrations average 473 ppm (Table 5).

The average grain size for sample P76610 is 120 μm. This sample has the fewest number of analyses that forms a discordant array, with the lower intercept giving a $^{206}Pb/^{238}U$ date of 120.6 ± 4.4 Ma (MSWD = 0.46) (Figure 9e; Table 4). Uranium and thorium concentrations in this sample are low, averaging 6.5 and 2.4 ppm, respectively (Table 5).

4.4 Zircon thermochronology

Ti-in-zircon temperatures were collected during SHRIMP analysis, and all errors calculated to 2σ; a summary of collected temperatures with associated dates can be found in Table 2. Analyses with high concentrations of Fe tended to yield temperatures with higher errors, as well as decrease the saturation of Ti in zircon; thus, analyses with Fe concentrations >> 100 ppm were excluded from temperature calculations (Table 3). Temperatures recorded in samples from Milford Sound, i.e., Arthur River Complex samples 15NZ58, 15NZ60, and 05NZ12P, are 756 ± 71 °C, 718 ± 62 °C, and 696 ± 27 °C, respectively (Table 2). These temperatures indicate that a granulite-facies metamorphic event must have occurred in the Arthur River Complex c. 135-126 Ma prior to WFO emplacement that caused these elevated temperatures (Table 2; see Discussion for further analysis). Samples 15NZ22 and 15NZ24B, both collected from Bligh Sound and George Sound Paragneiss, yielded temperatures of 827 ± 57 °C and 772 ± 52 °C, respectively (Table 2). Dates for George Sound Paragneiss in Bligh Sound are c. 120 Ma; these temperatures are consistent with syn-WFO high-temperature metamorphism of country rock (i.e., George Sound Paragneiss) during intrusion (Table 2; see Discussion for further analysis). The remaining samples were collected from George Sound Paragneiss outcrops in George Sound, and yielded temperatures of 819 ± 50 °C (15NZ7C), 767 ± 35 °C (15NZ11), 690 ± 20 °C (15NZ13), and 820 ± 21 °C (15NZ15) (Table 2). Much like in George Sound, these elevated temperatures are consistent with high-temperature metamorphism occurring due to the final stages of WFO intrusion into the George Sound Paragneiss from c. 121-116 Ma (Table 2; see Discussion for further analysis). Overall, temperatures obtained from these samples in northern Fiordland

varied between c. 690-830 °C, implying that all reached and exceeded granulite facies metamorphic conditions during c. 135-116 Ma (see Discussion for further analysis).

4.5 Titanite thermochronology

A summary of Zr-in-titanite temperatures, their 2σ errors, and their associated dates may be found in Table 4. In order to accurately interpret the temperatures, as well as dates, obtained by our titanite grains, traverses of grains were carried out during LASS-ICP-MS analysis (2-6 spots on large grains) (Figure 7a). On these traversed grains, a variety of dates with differences often spanning upwards of 10 Ma are collected; more often than not, these dates do not correspond to simple volume diffusion expectations (i.e., older cores, younger rims) (Figure 7a, 7b). If temperatures from titanite grains were simple closure temperatures, we would expect to see uniform ages throughout a single grain; however, this is not the case. Thus, we interpret the dates obtained for our titanite samples as the age of (re)crystallization during metamorphism, and the temperatures obtained as the associated temperature of formation (see Discussion for further analysis).

The northernmost titanite sample temperature comes from northeast of Sutherland Sound (P76610), with a temperature of 764 °C at c. 121 Ma (Table 4). Temperatures in Bligh Sound were variable, ranging between 753 °C at 103 Ma (15NZ22) and 929 °C at c. 105 Ma (15NZ24B) (Table 4). In the south, George Sound recorded temperatures of 837.3 °C at 94 Ma (15NZ15) and 762 °C at 112 Ma (P77080) (Table 4). Overall, metamorphic titanite temperatures ranged between c. 750-920 °C during c. 121-94 Ma.

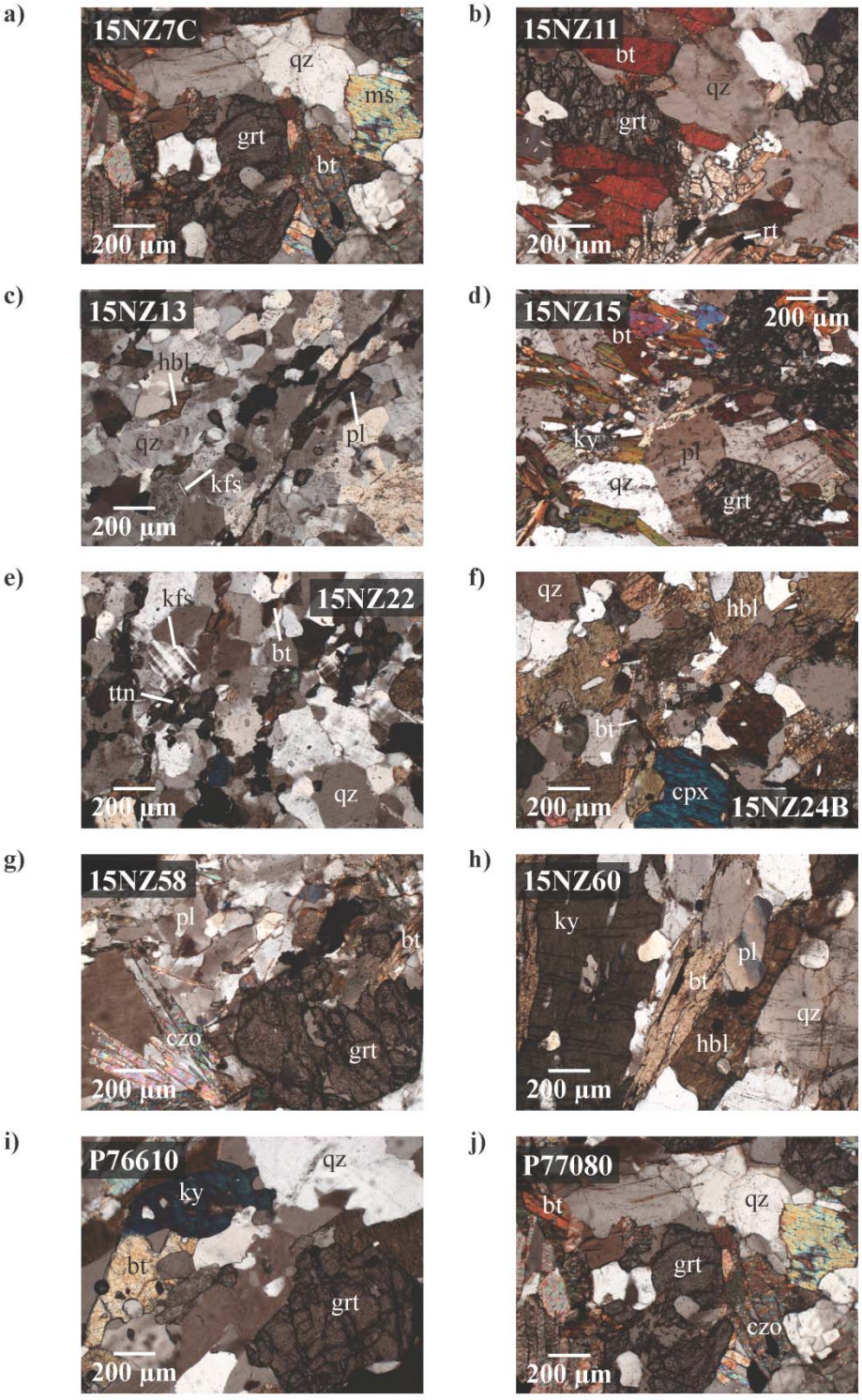

Figure 4: Representative petrographic photomicrographs showing mineral assemblages and textures present in each sample (excluding 05NZ12P). a) 15NZ7C; b) 15NZ11; c) 15NZ13; d) 15NZ15; e) 15NZ22; f) 15NZ24B; g) 15NZ58; h) 15NZ60; i) P76610; j) P77080. Abbreviations after Whitney and Evans (2010).

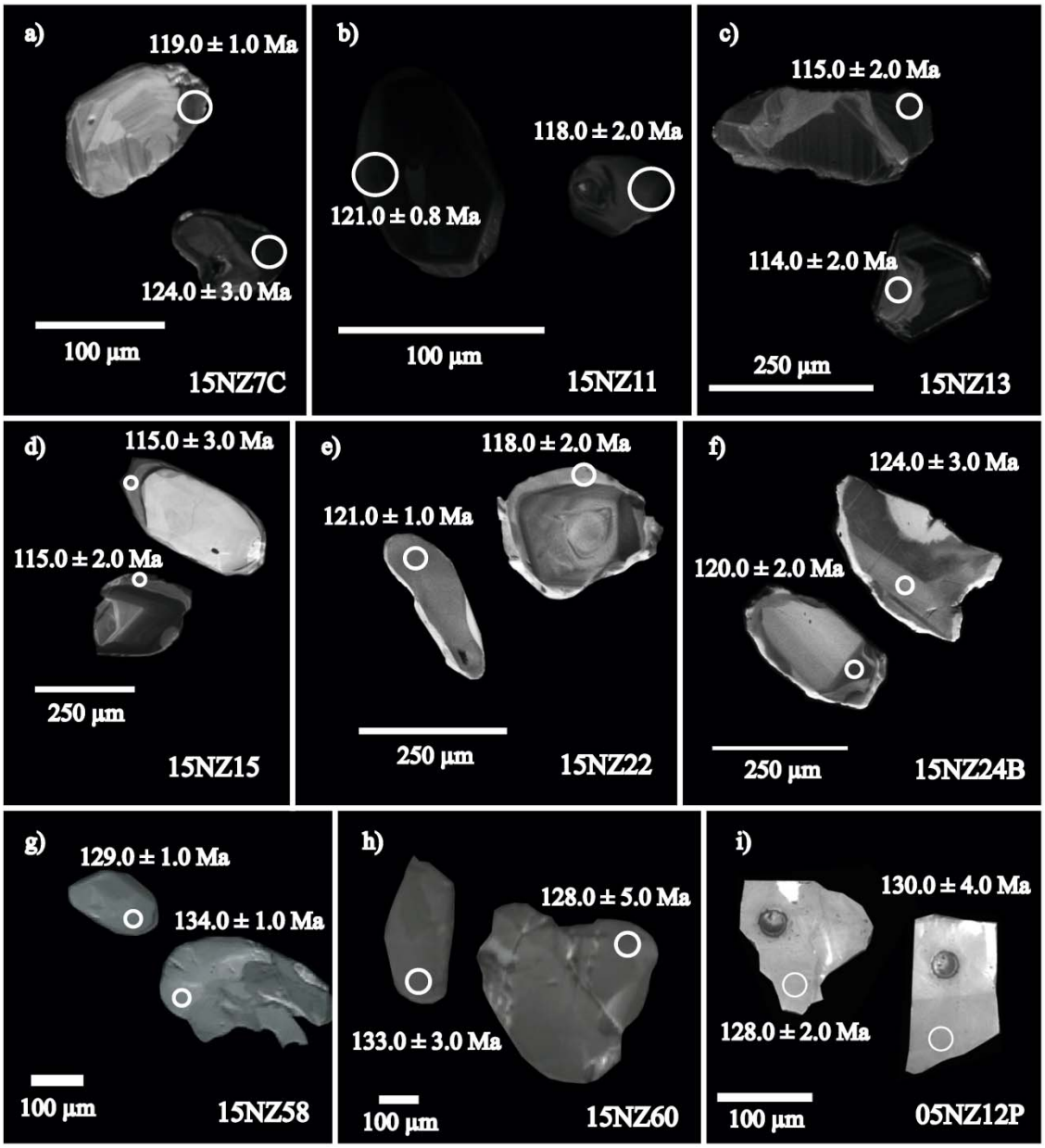

Figure 5: CL images of representative groups of metamorphic zircons from each sample, taken in order to avoid targeting inclusions and imperfections, as well as to aid in targeting metamorphic rims. (a) George Sound Paragneiss, George Sound (sample 15NZ7C), (b) George Sound Paragneiss, George Sound (sample 15NZ11), (c) George Sound Paragneiss, George Sound (sample 15NZ13), (d) George Sound Paragneiss, George Sound (sample 15NZ15), (e) George Sound Paragneiss, Bligh Sound (sample 15NZ22), (f) George Sound Paragneiss, Bligh Sound (sample 15NZ24B), (g) Harrison Creek Gneiss, Milford Sound (sample 15NZ58), (h) Selwyn Creek Gneiss, Milford Sound (sample 15NZ60), (i) Pembroke Granulite, Milford Sound (sample 05NZ12P). Pits show locations of LA-MC-ICPMS Lu-Hf spots (Decker et al., 2016). Note that this is a representative group of zircons; complete spots may be found in the Appendix.

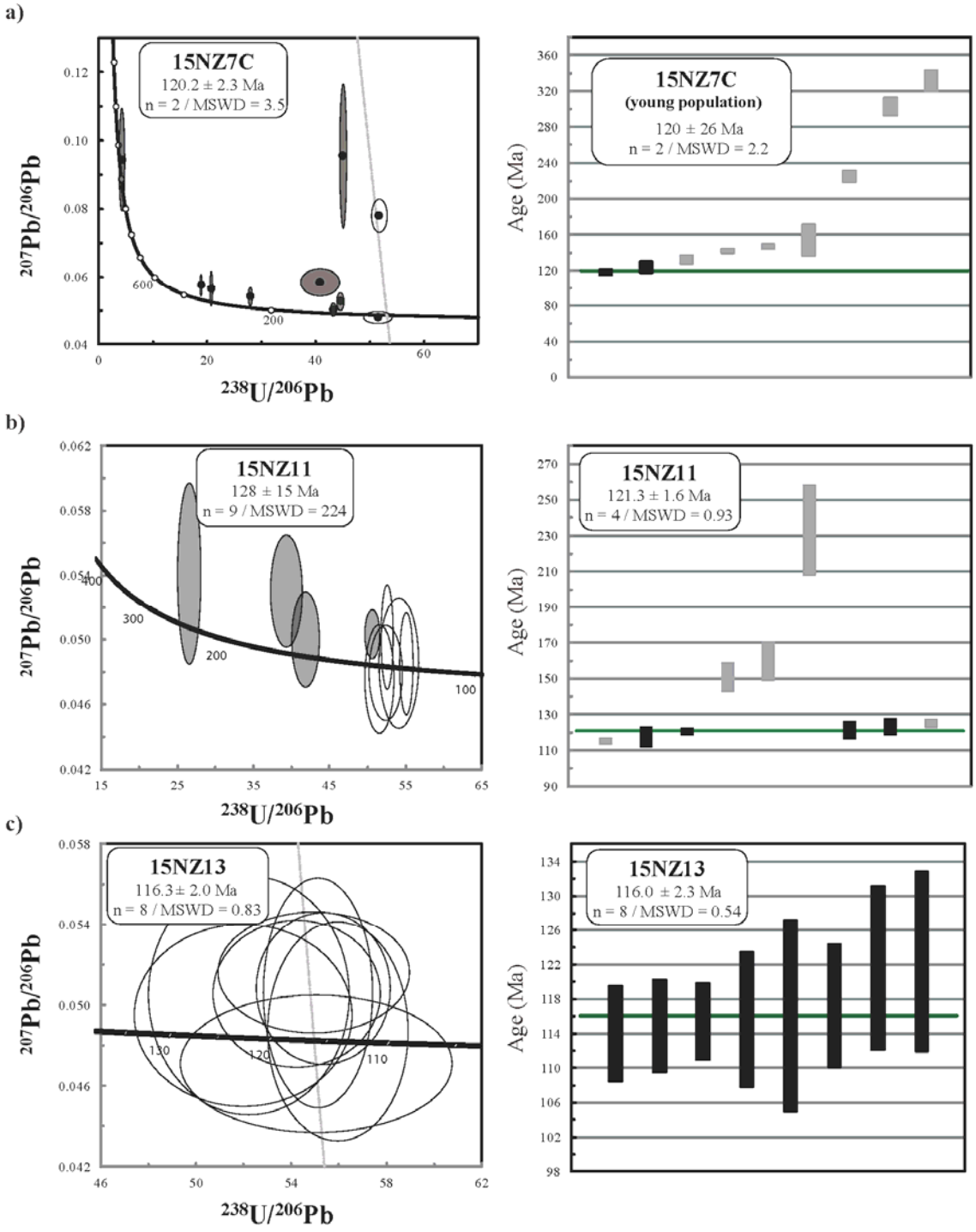
a)
15NZ7C
120.2 ± 2.3 Ma
n = 2 / MSWD = 3.5
600
200
$^{207}Pb/^{206}Pb$
$^{238}U/^{206}Pb$
15NZ7C
(young population)
120 ± 26 Ma
n = 2 / MSWD = 2.2
Age (Ma)
b)
15NZ11
128 ± 15 Ma
n = 9 / MSWD = 224
400
300
200
100
$^{207}Pb/^{206}Pb$
$^{238}U/^{206}Pb$
15NZ11
121.3 ± 1.6 Ma
n = 4 / MSWD = 0.93
Age (Ma)
c)
15NZ13
116.3± 2.0 Ma
n = 8 / MSWD = 0.83
130
120
110
$^{207}Pb/^{206}Pb$
$^{238}U/^{206}Pb$
15NZ13
116.0 ± 2.3 Ma
n = 8 / MSWD = 0.54
Age (Ma)

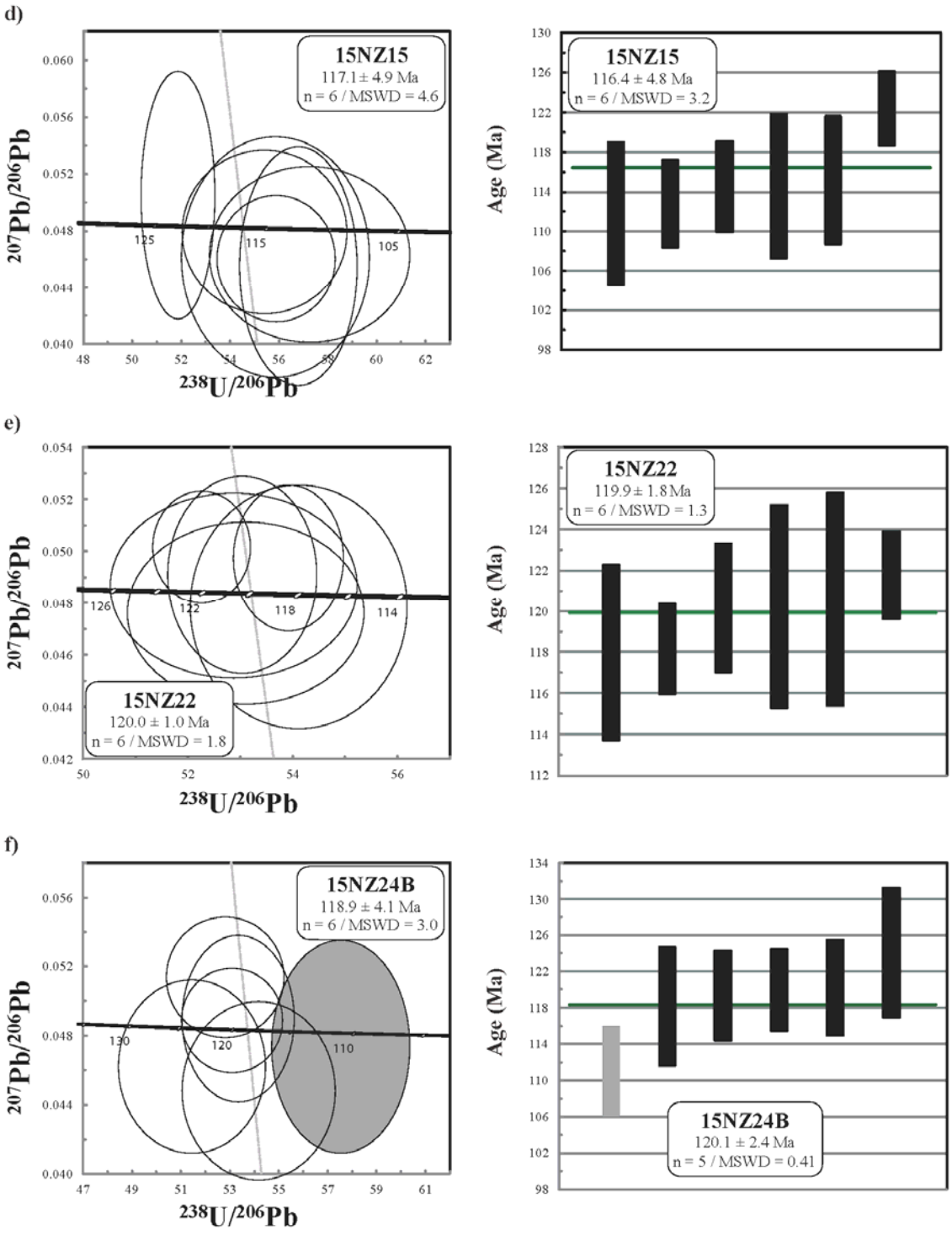
d)
15NZ15
117.1 ± 4.9 Ma
n = 6 / MSWD = 4.6
125
115
105
$^{207}Pb/^{206}Pb$
$^{238}U/^{206}Pb$
15NZ15
116.4 ± 4.8 Ma
n = 6 / MSWD = 3.2
Age (Ma)
e)
15NZ22
120.0 ± 1.0 Ma
n = 6 / MSWD = 1.8
126
122
118
114
15NZ22
119.9 ± 1.8 Ma
n = 6 / MSWD = 1.3
f)
15NZ24B
118.9 ± 4.1 Ma
n = 6 / MSWD = 3.0
130
120
110
15NZ24B
120.1 ± 2.4 Ma
n = 5 / MSWD = 0.41

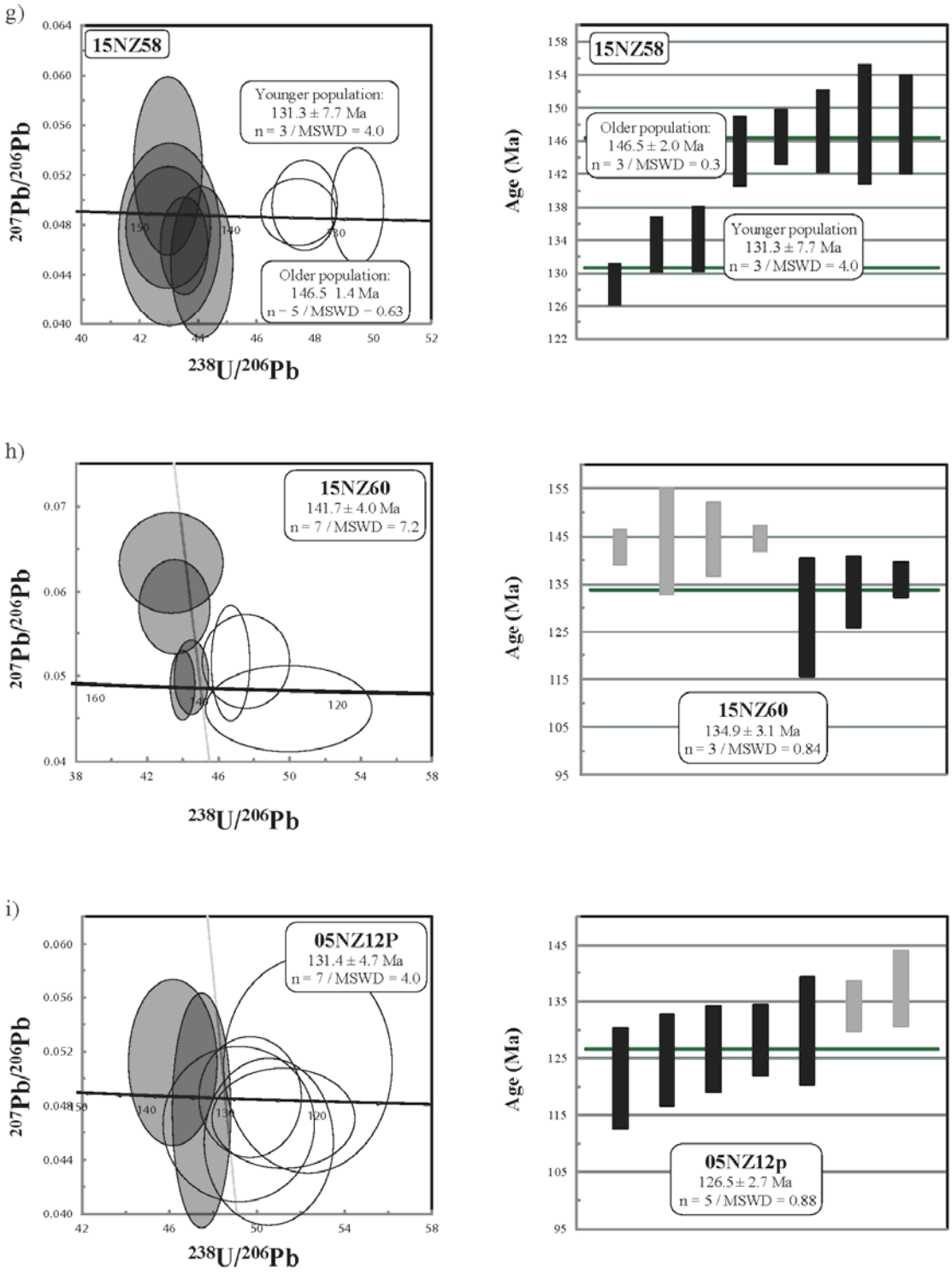

Figure 6: Tera-Wasserburg concordia plots and weighted average plots of SHRIMP-RG U-Pb zircon data for (a) 15NZ7C, (b) 15NZ11, (c) 15NZ13, (d) 15NZ15, (e) 15NZ22, (f) 15NZ24B, (g), 15NZ58, (h) 15NZ60, (i) 05NZ12P. All data point error ellipses are 2σ; all error bars are 2σ.

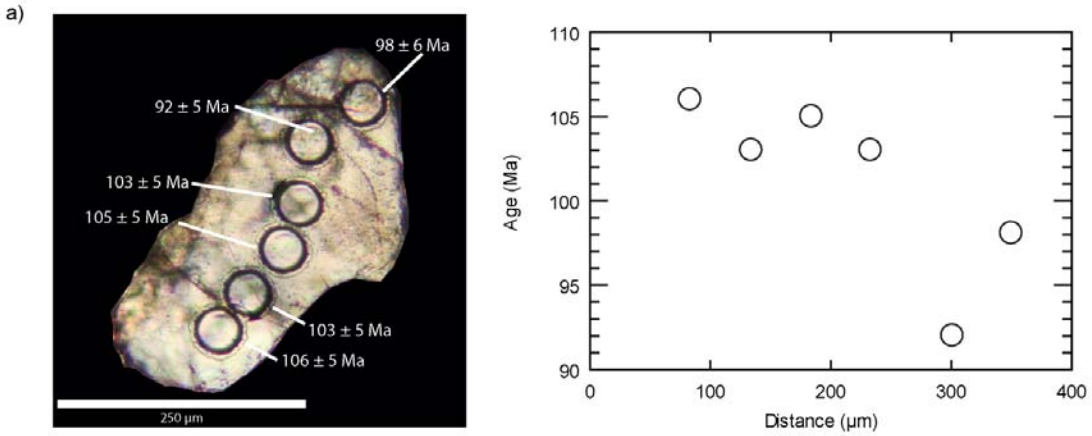

Figure 7: a) Example traverse of a titanite grain from sample 15NZ24B (George Sound Paragneiss, Bligh Sound). Spot size is 40 µm. Errors are 2σ (internal). b) Age v. distance plot for same titanite grain. Dates obtained are neither uniform nor show an expected core-rim pattern. Thus we interpret titanite dates as recording the temperature of a metamorphic event.

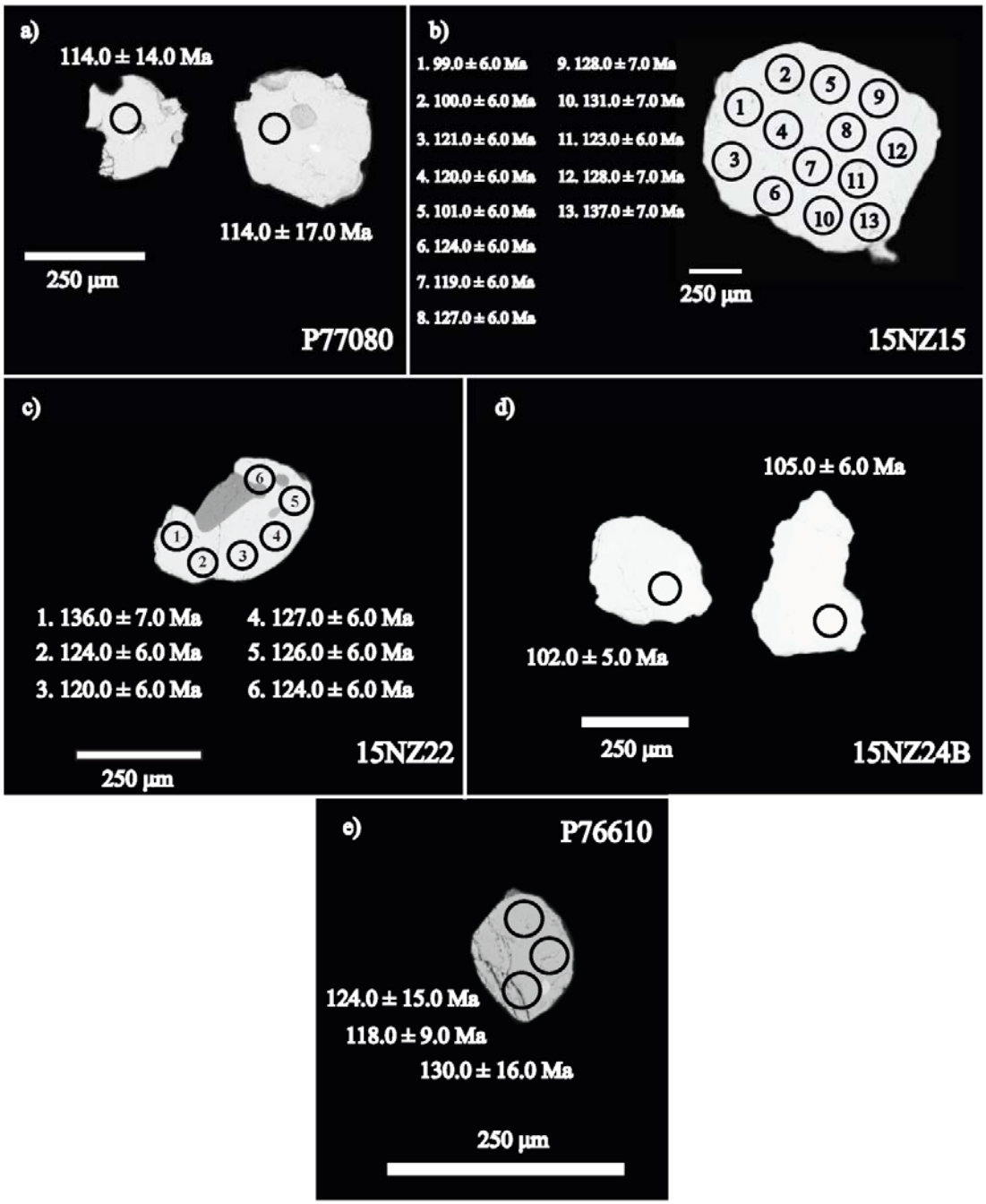

Figure 8: BSE images of representative titanite grains, used in order to avoid targeting inclusions and imperfections. (a) McKerr Intrusives, granodiorite, south of George Sound (sample P77080), (b) George Sound Paragneiss, George Sound (sample 15NZ15), (c) George Sound Paragneiss, Bligh Sound (sample 15NZ22), (d) George Sound Paragneiss, Bligh Sound (sample 15NZ24B), (e) Worsley Pluton, granodiorite, east of Sutherland Sound (sample P76610). Note that this is a representative group of titanite grains; all spots can be found in the Appendix.

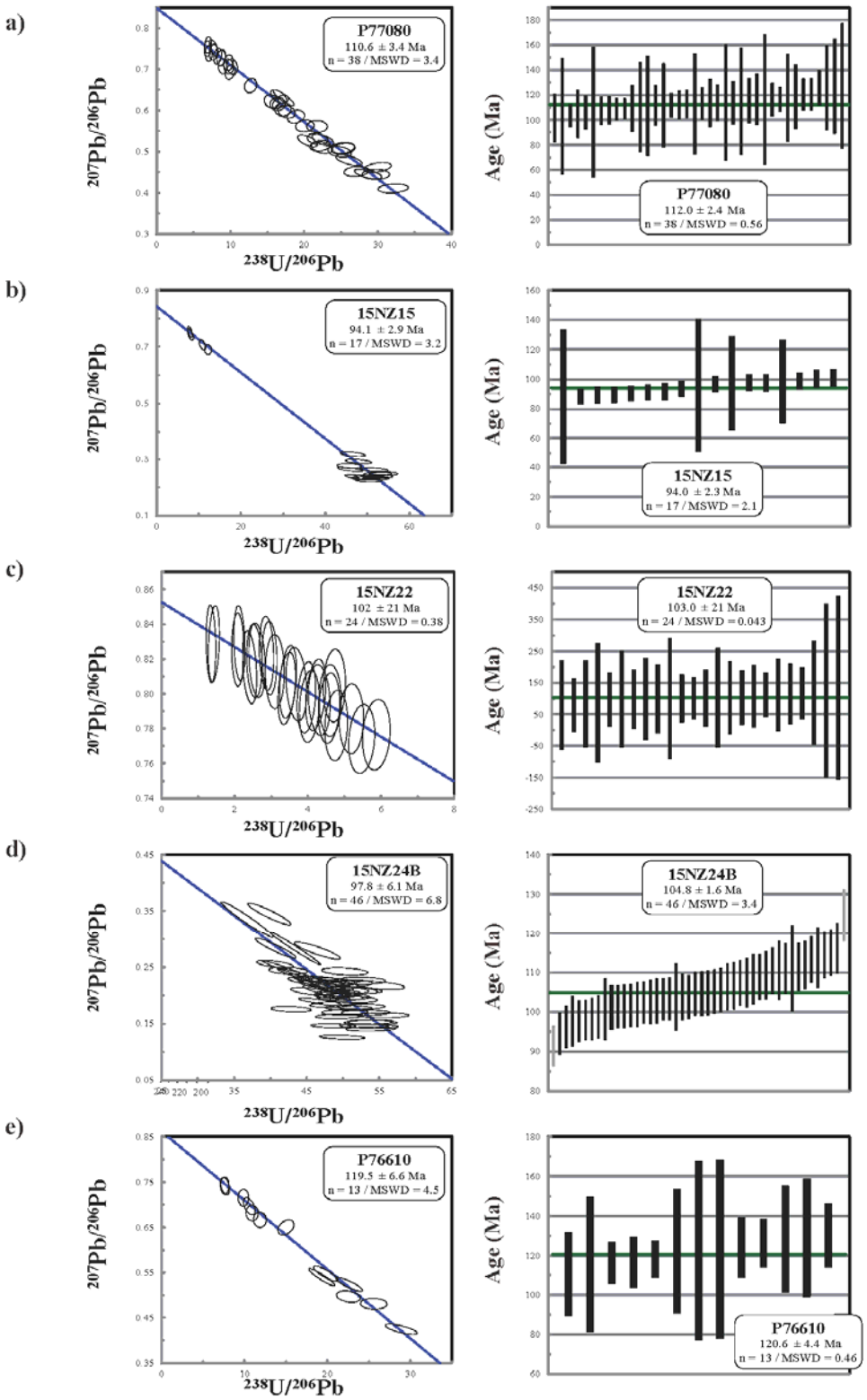

Figure 9: Tera-Wasserburg concordia plots and weighted average plots of LASS-ICP-MS U-Pb titanite data for (a) P77080, (b) 15NZ15, (c) 15NZ22, (d) 15NZ24B, (e) P76610. All data point error ellipses are 2σ; all error bars are 2σ.

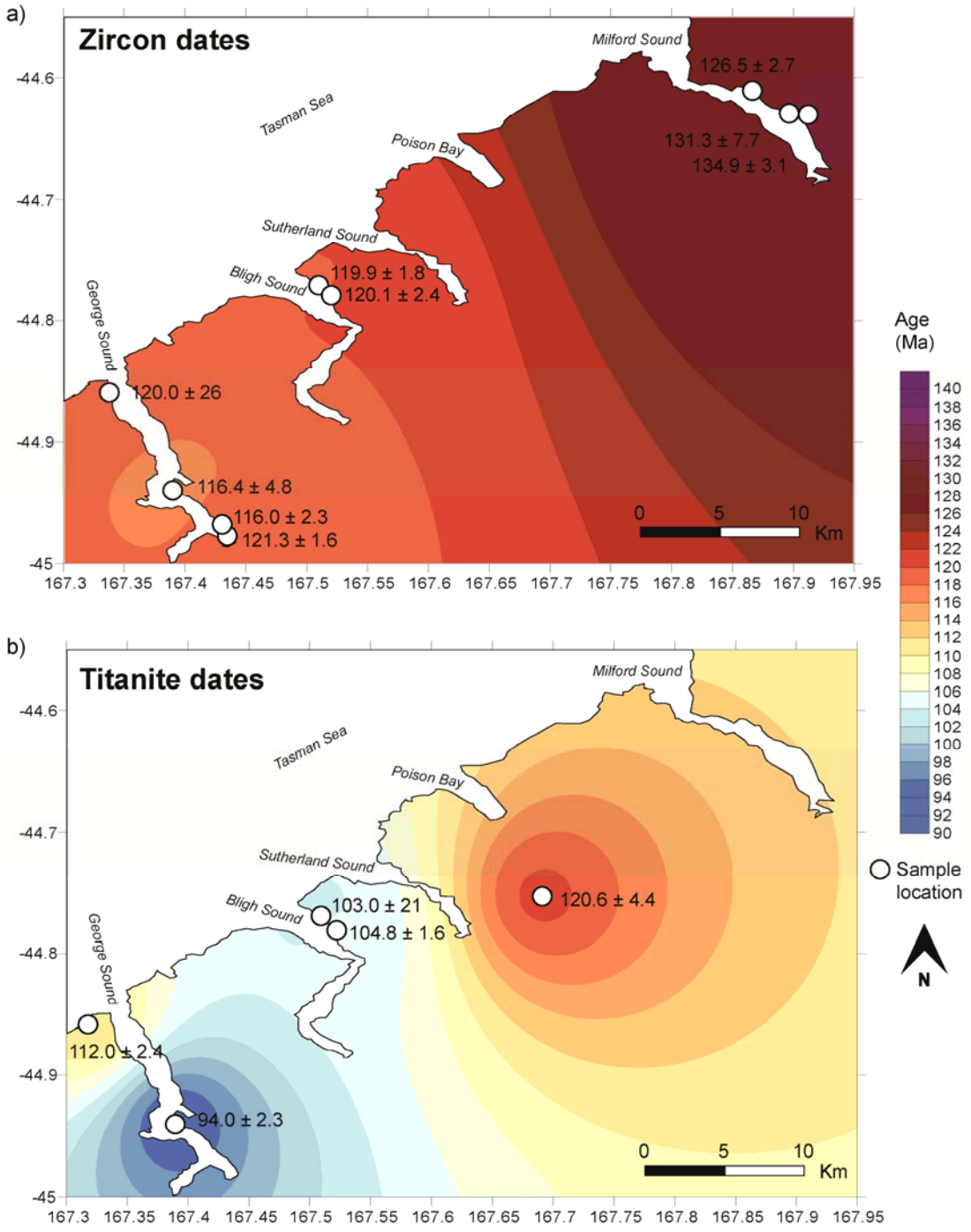

Figure 10: a) Inverse distance weighted (IDW) interpolation of zircon dates obtained during this study. The assigned values to the unknown points are calculated with a weighted average of the values at known points. b) : IDW interpolation of titanite dates obtained during this study.

Table 1: Summary of location and petrology of samples

Sample	Location	Unit	Rock type	Description	Mineral assemblage and abundance (%)
15NZ7C	George Sound	George Sound Paragneiss	Paragneiss	Moderate foliation, medium grained	Qz (40), bt (23), ms (15), pl (13), grt (10); rt, zrn, ilm (trace)
15NZ11	George Sound	George Sound Paragneiss	Paragneiss	Bimodal grain size; weak to moderate foliation	Qz (60), bt (12), pl (8), grt (7), opx (7), sil (6); rt, zrn (trace)
15NZ13	George Sound	George Sound Paragneiss	Paragneiss	Fine grained, weak to moderate foliation	Qz (57), pl (21), kfs (10), hbl (6), ky (4), ttn (2); zrn, grt, ilm (trace)
15NZ15	George Sound	George Sound Paragneiss	Paragneiss	Fine to medium grained, moderate foliation	Qz (45), grt (16), pl (15), bt (14), hbl (7), ky (2), rt (1); ttn, zrn (trace)
15NZ22	Bligh Sound	George Sound Paragneiss	Paragneiss	Moderate foliation, fine grained, felsic	Qz (47), pl (25), kfs (9), bt (8), hbl (5), ilm (4), ttn (2), zrn (trace)
15NZ24B	Bligh Sound	George Sound Paragneiss	Paragneiss	Moderate foliation, fine grained, felsic	Qz (43), hbl (27), pl (10), opx (9), ttn (6), cpx (3), bt (2); zrn, ilm (trace)
15NZ58	Milford Sound	Harrison Orthogneiss	Orthogneiss	Coarse grained, banded dioritic gneiss	Hbl (52), pl (22), qz (10), bt (5), czo (5), grt (3), ttn (2), rt (1), zrn (trace)
15NZ59	Milford Sound	Selwyn Creek Gneiss	Orthogneiss	Weak foliation, medium to coarse grained	Qz (34), hbl (30), pl (21), ky (8), bt (7); rt, zrn (trace)
05NZ12P	Milford Sound	Pembroke Granulite	Granulite	Garnet leucosome, dioritic gneiss	Hbl, cpx, pl, bt, czo, grt (see Stowell et al., 2010)
P76610	E. of Sutherland Sound	Worsley Pluton	Granodiorite	Moderate foliation, medium to coarse grained	Qz (44), bt (19), pl (15), ky (11), grt (6), czo (5); ttn, zrn (trace)
P77080	S. of George Sound	McKerr Intrusives	Granodiorite	Moderate foliation, fine to medium grained	Qz (45), pl (21), hbl (20), bt (8), czo (4), grt (2); ttn, rt, zrn (trace)

Table 1: Sample locations and petrographic descriptions. Mineral abbreviations are as follows (after Whitney and Evans, 2010): bt – biotite; cpx – clinopyroxene; czo – clinozoisite; grt – garnet; hbl – hornblende; ilm – ilmenite; kfs – potassium feldspar; ky – kyanite; ms – muscovite; opx – orthopyroxene; pl – plagioclase; qz – quartz; rt – rutile; sil – sillimanite; ttn – titanite; zrn – zircon.

Table 2: Summary of U-Pb zircon date and temperature data

Sample	Location	Zircon age (Ma)	Error (2σ)	MSWD	Temperature (°C)	Error (C°, 2σ)
15NZ7C	George Sound	120.0	26	2.2	819	50
	LA-ICP-MS date	121.3	2.3	0.36		
15NZ11	George Sound	121.3	1.6	0.93	767	35
15NZ13	George Sound	116.0	2.3	0.54	690	20
15NZ15	George Sound	116.4	4.8	3.2	820	21
15NZ22	Bligh Sound	119.9	1.8	1.3	827	57
15NZ24B	Bligh Sound	120.1	2.4	0.41	772	52
15NZ58	Milford Sound	131.3	7.7	4	756	71
15NZ60	Milford Sound	134.9	3.1	0.84	718	62
05NZ12P	Milford Sound	126.5	2.7	0.88	696	27

Table 2: Summary of U-Pb SHRIMP-RG zircon dates and associated temperatures. Complete isotopic data and individual spot dates can be found in the Appendix.

Table 3: SHRIMP-RG zircon trace element concentrations, ppm

Sample - spot	U	Th	48Ti	49Ti	Fe	Th/U
15NZ7C-1.1	500	27	502.4	474.2	983.0	0.056
15NZ7C-2.1	481	25	9.0	8.4	8.1	0.055
15NZ7C-3.1	71	54	11.8	11.4	4.4	0.779
15NZ7C-3.2	278	10	124.7	123.9	363.6	0.036
15NZ7C-4.1	355	25	6.9	6.6	4.1	0.073
15NZ7C-5.1	1232	39	6.9	6.8	5.9	0.033
15NZ7C-6.1	1310	12	10.1	9.9	1.9	0.010
15NZ7C-7.1	336	35	8.6	8.2	17.3	0.107
15NZ7C-8.1	435	151	10.9	9.8	4.9	0.359
15NZ7C-9.1	218	69	13.3	12.8	28.8	0.325
15NZ11-1.2	1882	41	6.9	6.8	8.4	0.020
15NZ11-2.1	1665	15	9.7	9.5	11.9	0.009
15NZ11-6.1	1073	7	6.9	6.5	1.2	0.007
15NZ11-7.1	558	7	6.7	6.6	6.0	0.014
15NZ11-11.1	1349	12	6.5	6.3	0.2	0.010
15NZ11-12.1	178	0	2.9	3.0	0.6	0.000
15NZ11-13.1	789	18	3.4	3.4	9.1	0.020
15NZ11-14.1	934	43	6.9	6.2	1.0	0.050
15NZ11-15.1	619	9	4.7	4.6	0.1	0.020
15NZ11-16.1	948	15	7.7	7.7	0.5	0.020
15NZ11-17.1	922	246	4.8	4.5	1.5	0.280
15NZ13-1.1	471	53	2.4	2.5	5.7	0.116
15NZ13-2.1	360	131	3.0	3.0	11.2	0.375
15NZ13-3.1	505	61	2.3	2.4	10.2	0.125
15NZ13-4.1	636	74	2.7	2.6	12.7	0.121
15NZ13-5.1	288	55	2.5	2.6	7.9	0.196
15NZ13-6.1	503	61	2.2	2.4	5.8	0.126
15NZ13-7.1	246	56	5.1	5.3	11.4	0.237
15NZ13-8.1	425	191	3.1	3.1	6.0	0.464
15NZ13-9.1	153	72	2.8	2.7	6.4	0.490
15NZ15-1.1	69	52	9.3	9.4	1.3	0.779
15NZ15-2.1	197	83	8.9	8.9	5.1	0.438
15NZ15-3.1	156	48	10.0	9.7	1.9	0.319
15NZ15-4.1	251	96	11.2	11.1	2.4	0.397
15NZ15-5.1	73	50	11.2	11.3	1.2	0.705
15NZ15-6.1	138	34	10.8	10.8	2.1	0.256
15NZ22-1.1	183	52	16.4	15.8	162.4	0.295
15NZ22-2.1	845	688	8.6	8.3	11.6	0.841
15NZ22-3.1	497	223	11.5	11.2	17.1	0.463
15NZ22-4.1	374	286	8.4	8.1	5.5	0.790
15NZ22-5.1	349	110	9.5	9.1	9.8	0.327

15NZ22-6.1	323	97	12.7	12.6	4.7	0.312
15NZ24b-1.1	1419	496	5.8	5.7	12.8	0.361
15NZ24b-2.1	1155	333	3.4	3.4	12.5	0.298
15NZ24b-3.1	399	145	5.8	5.7	7.6	0.376
15NZ24b-4.1	277	99	1.2	1.2	6.7	0.369
15NZ24b-5.1	6	2	0.6	0.6	0.4	0.386
15NZ24b-6.1	447	165	6.2	6.4	5.5	0.383
15NZ24b-7.1	1	0	0.4	0.4	0.2	0.198
15NZ24b-8.1	986	466	14.0	14.2	3.4	0.488
15NZ24b-9.1	1	0	0.4	0.4	0.3	0.106
15NZ58-1.1	1783	119	2.2	2.2	24.0	0.069
15NZ58-2.1	136	65	8.7	8.8	5.0	0.495
15NZ58-3.1	331	347	14.6	14.3	11.9	1.082
15NZ58-4.1	1008	836	7.5	7.5	22.5	0.858
15NZ58-5.1	608	682	9.1	9.4	14.6	1.159
15NZ58-6.1	247	126	8.4	7.9	15.2	0.529
15NZ58-7.1	154	102	8.5	8.5	4.7	0.687
15NZ58-8.1	181	78	3.7	3.7	0.6	0.447
15NZ58-9.1	129	65	8.0	8.1	4.7	0.517
15NZ60-3.1	246	46	1.5	1.5	2.3	0.190
15NZ60-4.1	221	52	6.6	6.4	35.4	0.240
15NZ60-5.2	126	52	2.8	2.8	1.2	0.430
15NZ60-5.3	176	34	5.3	5.1	7.8	0.200
15NZ60-6.2	195	40	1.7	1.7	1.4	0.210
15NZ60-7.1	284	145	3.1	3.0	2.7	0.530
15NZ60-8.1	154	26	1.7	1.6	1.1	0.170
15NZ60-10.1	269	170	21.8	22.1	185.3	0.650
05NZ12p-2.3	80	42	5.91	5.95	0.4	0.549
05NZ12p-4.3	160	132	12.34	12.33	0.4	0.854
05NZ12p-5.3	97	70	2.45	2.38	1.4	0.747
05NZ12p-7.3	214	167	3.13	3.11	4.2	0.807
05NZ12p-8.3	333	310	3.16	3.08	2.6	0.962
05NZ12p-9.3	150	123	2.28	2.33	1.6	0.842
05NZ12p-10.2	463	443	3.13	3.08	9.7	0.990

Table 3: Summary of relevant trace elements and trace element ratios in zircon samples. A complete table of trace and rare earth element concentrations can be found in the Appendix.

Table 4: Summary of U-Pb titanite date and temperate data

Sample	Location	Titanite age (Ma)	Error (2σ)	MSWD	Temperature (°C)	Error (C°, 2σ)
P77080	S. of George Sound	112.0	2.4	0.560	762	50
15NZ15	George Sound	94.0	2.3	2.100	837	50
15NZ22	Bligh Sound	103.0	21	0.043	753	50
15NZ24B	Bligh Sound	104.8	1.6	3.400	929	50
P76610	E. of Sutherland Sound	120.6	4.4	0.460	764	50

Table 4: Summary of U-Pb LASS-ICP-MS titanite dates and associated temperatures. Complete isotopic data and individual spot dates can be found in the Appendix.

Table 5: Average LASS-ICP-MS titanite trace element concentrations, ppm

Sample	U	Th	Zr
P77080	13	11.6	187
15NZ15	24	60	710
15NZ22	2.84	0.58	157
15NZ24B	117	473	2590
P76610	6.5	2.4	78

Table 5: Summary of relevant trace elements in titanite samples. A complete table of trace and rare earth element concentrations can be found in the Appendix.

5. DISCUSSION

5.1 Thermal evolution of northern Fiordland and implications

Zircon geochronology yields several key observations regarding the thermal evolution of the arc root in northern Fiordland: 1) oldest metamorphic dates are located in the northern areas and from deeper paleodepths of the arc (i.e., Milford Sound), and younger dates are observed at the shallower paleodepths in the south (i.e., George Sound) (Klepeis et al., 2007) (Figure 10a, 10b); 2) the oldest phase of metamorphism predated WFO emplacement and occurred from c. 135-127 Ma in the Arthur River Complex in Milford Sound (Figure 10a); 3) a second phase of metamorphism occurred synchronously with the emplacement of the WFO into the mid to lower crust between c. 121-116 Ma (Mattinson et al., 1986; Hollis et al., 2003; Klepeis et al., 2003; Klepeis et al., 2007; Allibone et al., 2009) (Figure 10a, 10b); and 4) granulite facies metamorphic temperatures range between c. 830 to 690 °C and indicate that the lower crust remained hot prior to and during the emplacement of the WFO between c. 121-116 Ma.

Geochronology of titanite samples further illuminate the heating and cooling history of northern Fiordland but also reveal younger dates. Similar to zircon data, titanite dates in the lower pressure, shallow paleodepth region (i.e., George Sound) are younger than those in the higher pressure, deeper paleodepth region (i.e., Milford Sound) (Figure 10b). This temporal pattern is contrary to expectations for simple arc cooling, whereby the shallower parts of the arc would cool first (and thus give older ages), and the deeper part of the arc would cool last (and thus give younger ages). Titanite thermochronology also reveals elevated temperatures ranging between c. 920 – 750 °C. These temperatures indicate growth/recrystallization of titanite over c. 121-94 Ma, a period > 25 Ma and

imply that the crust in northern Fiordland remained at elevated temperatures (i.e., granulite facies metamorphic conditions) over a 40 Ma interval from c. 135-94 Ma. In the following, we discuss our interpretations of titanite thermochronology, place our work within the broader metamorphic and cooling history of northern Fiordland, and hypothesize various mechanisms that may be responsible for sustained lower crustal heating.

5.2 Interpreting titanite dates as ages of metamorphic (re)crystallization

The dates and corresponding temperatures obtained for titanite grains in this study elucidate a complex history of metamorphism and prolonged heating in the lower crust of northern Fiordland. Grain traverses were conducted on large grains (>200 μm in length) in an effort to gain insight into their growth history (e.g., Figure 7a; Figure 8b, c, e). Titanites showed no age pattern indicative of simple cooling and volume diffusion (e.g., Cherniak, 2010). Cores of grains, expected to grow/cool first, are frequently younger than rims and vise versa (Figure 7a, 7b; Figure 8b, 8c, 8e). Additionally, dates ranges on individual grains often vary by >10 Ma, contrary to the uniform age distribution expected with volume diffusion. For example, a grain from sample 15NZ15 has spots with dates ranging from 99.0 ± 6.0 to 137.0 ± 7.0 Ma, a span of ~38 Ma (Figure 8b). Moreover, the oldest spot is located along the edge of the grain, which is also inconsistent with Pb mobility controlled by the volume diffusion process. These observations demonstrate that volume diffusion is unlikely to be the dominant process occurring in these titanite samples.

Previous thermochronologic studies in Fiordland have interpreted titanite dates to represent the time at which the arc crust cooled through a closure temperature of c. 600-

650 °C (e.g., Flowers et al., 2005) (Table 4). Following this assumption, Flowers et al. (2005) interpreted titanite dates to indicate rapid cooling from magmatic temperatures through c. 600 °C in ~6 Ma. In contrast, Schwartz et al. (in press) observed that the lower crust in central Fiordland remained hot (> 800 °C) through c. 108 Ma well after the high flux event that emplaced the WFO between 124-115 Ma (Gibson and Ireland, 1995; Hollis et al., 2004; Klepeis et al., 2004). Zircon and titanite thermochronology in this study are consistent with the concept of persistent high temperatures in the lower crust of Fiordland during episodic metamorphic growth and/or (re)crystallization resulting from fluid flow in the lower crust. These studies, along with our data, call into question the validity of interpreting titanite dates as representing the age of passing through a fixed closure temperature.

The Zr-in-titanite temperatures estimated in this study depend on several variables, as explicitly stated in equation 7 of Hayden et al. (2008) from which our calculations derive, namely pressure, TiO_2 and SiO_2 activities, and Zr concentration. As previously discussed, the pressures assigned to each sample derive from values from Klepeis et al. (2007) that best corresponded to the geographic locations of our samples. Activities of SiO_2 and TiO_2 were assumed at 1 because of the presence of quartz and rutile and/or ilmenite in all samples (Hayden et al., 2008). Additionally, because Zr can replace Ti in titanite grains, titanites are generally quite retentive of Zr; even for rutile absent assemblages, the average Zr content does not statistically differ (Hayden et al., 2008). Given the above observations, we interpret our titanite dates to reflect the age and temperature at which metamorphic (re)crystallization occurred in association with emplacement of the WFO into the mid-to-lower crust in northern Fiordland. Our titanite

thermochronology demonstrates that the lower crust in northern Fiordland remained hot, recording temperatures between 920-750 °C, during and after WFO emplacement from c. 121-94 Ma. Together, with zircon thermochronology, the results show that the lower crust remained hot and weak for > 40 Ma.

5.3 Arc evolution and metamorphism in northern Fiordland

Figure 11 synthesizes date and temperature data from this and other thermochronologic studies of northern Fiordland, and compares data from the north to the time-temperature path synthesized by Schwartz et al. (in press) for central Fiordland. Here, we place our data in context of previous studies to elucidate the complexities present within the changing tectonic environment of Zealandia occurring approximately between 135 Ma and 94 Ma.

5.3.1 Pre-WFO emplacement (> 125 Ma)

Metamorphism occurring prior to the emplacement of the WFO is recorded in the Arthur River Complex in this as well as previous studies (e.g., Clarke et al., 2000; Hollis et al., 2003; Stowell et al., 2010; Tulloch et al., 2011). The three oldest metamorphic zircon dates obtained by this study are from Arthur River Complex samples – 15NZ60 (Selwyn Creek orthogneiss), 15NZ58 (Harrison Creek orthogneiss), and 05NZ12P (Pembroke Granulite) (Table 2). Dates from these samples range between c. 134 – 126 Ma, and corresponding temperatures range between 756 – 696 °C (Table 2; Figure 11). We interpret these Pb/U dates as metamorphic because of older core dates for the Harrison and Selwyn Creek gneisses obtained by Decker et al. (unpub.) of c. 146 and 179 Ma, respectively. These dates agree with a granulite-facies metamorphism event occurring c. 134 Ma in the Arthur River Complex identified by previous studies likely to

have been caused by tectonic accretion (Stowell et al., 2010; Tulloch et al., 2011). The c. 134 Ma metamorphic event also coincides with a low period of Median Batholith magmatism, which has been suggested to have been caused by a thermal event in the deep crust that shortly afterward caused the high-flux event that emplaced the WFO/SPS (Tulloch et al., 2011). Sm-Nd dates from Stowell et al. (2010) records garnet growth in the Pembroke Granulite at ~126 Ma and ~850 °C as a response to high-pressure granulite facies metamorphism likely induced by partial melting before the emplacement of the WFO (Figure 11) Further, P-T data from Daczko et al., 2002 suggests the persistence of granulite-facies conditions (T = 750-850 °C) in the Arthur River Complex during convergence was due to partial melting during this time.

5.3.2 Syn-WFO emplacement (125-115 Ma)

Emplacement of mafic to intermediate magmas into the mid to lower crust in Fiordland resulted in high temperature metamorphic conditions in the contact aureole of the WFO (Clarke et al., 2000; Hollis et al., 2003; Stowell et al., 2010). Previous studies have dated the emplacement of the WFO between c. 125-115 Ma, which reflects the terminal pulse of Median Batholith magmatism (Mattinson et al., 1986; Hollis et al., 2003; Klepeis et al., 2003; Klepeis et al., 2007; Allibone et al., 2009; Schwartz et al., in press). Metamorphic zircons from the George Sound Paragneiss host in George and Bligh Sounds demonstrate contemporaneous metamorphism during WFO intrusion (Figure 11; Table 2). Our data yield metamorphic zircons dates between c. 121 and 116 Ma at temperatures between 827 – 690 °C (Figure 11; Table 2). These metamorphic zircon dates are supported by a titanite date of 120.6 Ma (T = 765 °C) from the Worsley Pluton (Figure 11; Table 4). Garnet growth at 122.6 Ma and 850 °C also occurred concurrently

with metamorphic zircon and titanite growth during initial WFO intrusion (Stowell et al., 2010). Additionally, Flowers et al. (2005) reported a titanite date of c. 120 from a mafic granulite in Milford Sound. These dates, along with our other metamorphic zircon and titanite dates, reflect metamorphic growth that occurred during WFO magmatism and may be related to tectonic collision-related burial of the WFO in Fiordland by ~25 km of continental crust (Bradshaw, 1990; Clarke et al., 2000; Hollis et al., 2004; Flowers et al., 2005; Allibone et al., 2009).

5.3.3 Post-WFO emplacement

Following the cessation of WFO magmatism, sustained high-temperature granulite facies metamorphic conditions are recorded by the growth / (re) crystallization of titanite grains in this study, as well as garnet growth as documented in previous studies (i.e., Stowell et al., 2010). Titanites from the eastern McKerr Intrusives south of George Sound (P77080) record a temperature of 762 °C at 112 Ma, shortly after the cessation of emplacement of the WFO (Figure 11; Table 4). These data point indicates continued granulite-facies metamorphic conditions within the WFO after intrusion. Three titanite dates from exposures of George Sound Paragneiss in Bligh and George Sounds indicate sustained high temperatures between 928 and 753 °C in the host country rock between at least c.105 and 94 Ma (Figure 11; Table 4). These data agree with Sm-Nd garnet data from a Pembroke Granulite garnet reaction zone (Arthur River Complex), which gives an age of c. 108 Ma and temperature of ~850 °C (Stowell et al., 2010; Figure 11). A plausible interpretation for this garnet date is slow cooling of the host rock and/or late garnet growth (Stowell et al., 2010). Other garnets from Stowell et al. (2010) give dates of c. 94 Ma, which agree with our 94 Ma titanite date (T = 837 °C; from George Sound).

These dates substantiate the existence of sustained (re)heating or slow cooling taking place in the lower crust.

5.4 Tectonic and non-tectonic processes to sustain post-emplacement heating

Data from this study demonstrate that the last pulses of Median Batholith magmatism engendered elevated temperatures in the lower crust of northern Fiordland. Though while not "strong and cold" (T < 700 °C) as predicted by previous studies (e.g., Klepeis et al., 2004; Klepeis et al., 2007), northern Fiordland lacks comparable extensional features observed in central Fiordland which facilitate fluid flow and sustained elevated temperatures (Klepeis et al., 2004; Klepeis et al., 2007; Schwartz et al., in press). In the following sections we speculate about the contributions of various tectonic and non tectonic mechanisms which may explain the prolonged heating history of > 40 Ma which our data elucidate for northern Fiordland.

5.4.1 Delamination, extension, and thermal evolution

Delamination, or foundering, of a dense arc root, a driven by the formation of a density instability, can contribute to prolonged elevated temperatures observed in the lower crust (Figure 12; Lee, 2014). A dense, mafic arc root can form in a number of ways – via magmatic underplating, crystal accumulation, or concentration of melt depletion residues (Lee, 2014). An instability which leads to foundering can arise due to the density difference between the mafic root, the comparatively less dense upper crust and the underlying hot mantle (Lee, 2014). Once foundering is initiated, hot asthenosphere upwells to fill the void, which allows for lithospheric melting and contemporaneous elevated temperatures at or near the surface (Lee, 2014). Foundering can also cause isostatic rebound and small volumes of basaltic magmatism (Lee, 2014).

Since dense arc roots typically founder if underlain by hot (> 800 °C) lithospheric mantle (Lee, 2014), we believe that the elevated temperatures that persisted after the emplacement of the WFO (c. 112-94 Ma) in northern Fiordland were at least partially due to the foundering of a dense arc root. Klepeis et al. (2016) found that a dense, garnet pyroxenite lower crustal root formed at depths of ~40-65 km in Fiordland by c. 123 Ma, with the flare-up which emplaced the WFO rejuvenating the base of the arc and causing crustal melting and granulite-facies metamorphism. The flow of lower crustal melt caused by the WFO emplacement formed two gneissic domes in central Fiordland –the Breaksea and Malaspina (Klepeis et al., 2016). Both these domes record changing flow styles c. 114 Ma, facilitating the persistence of a hot, weak lower crust which in turn facilitated the foundering of the dense lower crustal root (Klepeis et al., 2016). Further, the foundering of the arc root at this time likely drove lower crustal thinning in Fiordland prior to the onset of upper crustal extension as recorded in central Fiordland (e.g., Doubtful Sound Shear Zone, Resolution Island Shear Zone; Klepeis et al., 2016). The foundering of this root undoubtedly contributed to elevated temperatures in Fiordland (e.g., titanites recording elevated temperatures in this study at c. 112 Ma and T = 750-930 °C), as well as associated upwelling-related magmatism in the lower crust.

Hot, upwelling mantle heated the lower crust during crustal thinning and extension. Starting at 112 Ma, long-lived subduction ceased in Zealandia and rifting and extension began as the dominant tectonic regime until ≤ 82 Ma (Tulloch et al., 2009; Stowell et al., 2014; Klepeis et al., 2016; Schwartz et al., in press). Bradshaw (1989) proposed ridge subduction as a means by which the tectonic regime changed from convergence to extension between 105 and 83 Ma in Zealandia; this hypothesis is

supported by A-type (anorogenic) magmatism occurring at c. 112 Ma in the Eastern Province (Tulloch et al., 2009). In central Fiordland, extensional orogenic collapse began from 108-106 Ma with the development of the Doubtful Sound Shear Zone (DSSZ), and continued to c. 88 Ma in the Breaksea area (Klepeis et al., 2016; Schwartz et al., in press). Extensional features which sustained heating in Fiordland became prevalent between 105-100 Ma (e.g., Bradshaw, 1989; Mortimer, 2008; Tulloch et al., 2009; Klepeis et al., 2016; Schwartz et al., in press). Additionally, widespread A-type magmatism occurred episodically in Fiordland and the entirety of Zealandia at c. 101, 97, and 83 Ma (Tulloch et al., 2009). This increase in A-type magmatism over time is likely due to crustal thinning throughout the region occurring during extension (Tulloch et al., 2009). Further, sustained heating in the Median Batholith allows a hotter, more ductile lithosphere to accommodate stretching via ductile flow; as a result, brittle fracturing and shearing moves inboard after 97 Ma, where the break up Gondwana eventually occurs (Tulloch et al., 2009; Klepeis et al., 2016).

5.4.2 Lower crust-mantle interactions

Emplacement of basalt (and thus heat) into the crust occurs primarily in the lower crustal MASH zone (Hildreth and Moorbath, 1988; Dufek and Bergantz, 2005). In order to better understand the protracted persistence of elevated temperatures obtained for northern Fiordland by this study, we consider the nature and effects of basaltic interaction with the lower crust. Dufek and Bergantz (2005) proposed that the primary mechanism through which the mantle interacts with the lower crust is through dike swarms. Successive dike emplacement increases the temperature, and thus also decreases the strength of the lower crust (Dufek and Bergantz, 2005). Since the strength of the lower

crust depends on its temperature, melt fraction, and fluid activity, it is reasonable to deduce that the emplacement of the WFO between c. 125-115 Ma thermally weakened the lower crust into which it intruded; further, its strength must have increased once fluids and melts cooled and/or migrated from it post emplacement c.116-105 Ma (Klepeis et al., 2003; Dufek and Bergantz, 2005). Previous work (e.g., Klepeis et al., 2003; Klepeis et al., 2007) demonstrates that in central Fiordland, diking and fracturing (e.g., shear zones) related to extension were essential in migrating mantle-derived basaltic melts, and thus also heat, out from the lower crust, as models from Dufek and Bergantz (2005) predict. Further research is needed to understand more clearly the dominant heat-sustaining mechanism in the lower crust, sustained by 1) extensional structural features not sampled nor documented in this study which recorded extensional orogenic collapse in northern Fiordland; and/or 2) lithospheric heating from the mantle due to foundering of a dense root (e.g., Klepeis et al., 2016).

5.5 Thermochronology of other lower crustal arc sections

In order to place these results within a broader context, we examine the metamorphic and cooling histories of other magmatic arcs throughout the world. These other magmatic arc sections demonstrate the myriad of tectonic and non-tectonic processes which can contribute to sustained elevated temperatures in the lower crust.

5.5.1 Western Gneiss Region, Norway

Kylander-Clark et al. (2008) examined the exhumation following subduction of an ultra-high pressure terrain in Western Gneiss Region (WGR), Norway, via U-Pb titanite and rutile thermochronology. Titanite dates range from c. 393-390 Ma, and rutile dates range from c. 392-385 Ma, with titanite from this region experiencing temperatures

of > 700 °C (Kylander-Clark et al., 2008). Post-peak pressure and temperature conditions in the WGR record two separate events: 1) exhumation from ~120 km depth to the mid-crustal depth (~20 km) in 12 Ma, and 2) cooling during tectonic unroofing and progressive slab exhumation from 600-800 °C to 400 °C (Kylander-Clark et al., 2008). For the first event, titanite dates allow for estimation of exhumation rate over ~12 Ma, which is calculated as 7 mm/yr; this is a slower rate than from nearby smaller terranes, but comparable to other larger terranes (Kylander-Clark et al., 2008). To constrain the latter event, differences between rutile and titanite dates and $^{40}Ar/^{39}Ar$ muscovite dates from this study imply a temperature drop from 750 °C to 400 °C in ~4 Ma, respectively, and thus a cooling rate of 90 °C /Ma during tectonic unroofing and progressive slab exhumation (Kylander-Clark et al., 2008). While the cooling rates observed in the WGR are faster than Fiordland, this study demonstrates the profound effect tectonic environment and events can have on metamorphic and cooling histories.

5.5.2 Sierra Nevada, California

The Sierra Nevada arc of California is a long-lived (> 140 Ma) magmatic arc that experienced at least two short-lived, voluminous episodes of magmatism which emplaced the Sierra Nevada batholith (Ducea, 2001). For the purposes of this discussion, we examine the last magmatic flare-up which occurred c. 100-85 Ma, prior to arc shut-off and the transition to flat slab Farallon plate subduction (Ducea, 2001; Chapman et al., 2013). Chapman et al. (2013) hypothesizes this late flare-up was caused first by the flattening of the slab during subduction, but more importantly by the subduction of hydrated metasediments into the MASH zone beneath the northern Sierran arc, which released volatiles and caused melting and "relamination" at the base of the lower crust.

This event must have allowed for sustained high temperatures in the Sierran arc, not unlike Fiordland, that lasted until and after the foundering of the dense arc root. The root that formed during relamination took ~70 Ma to be convectively removed, i.e., to founder, possibly because of "refrigeration" of the root by the shallow downgoing Farallon slab (Ducea, 2001; Saleeby et al., 2003; Chapman et al., 2013; Lee, 2014). The presence of continued high temperatures in the Sierran arc is substantiated by the occurrence of magmatism occurring in Late Miocene to Pliocene time (Saleeby et al., 2003). In Fiordland, there is no clear evidence supporting a similar flattening of a downgoing slab, though the presence of a foundering arc root could similarly explain elevated temperatures lasting beyond the occurrence of the last voluminous flare-up (i.e., WFO emplacement).

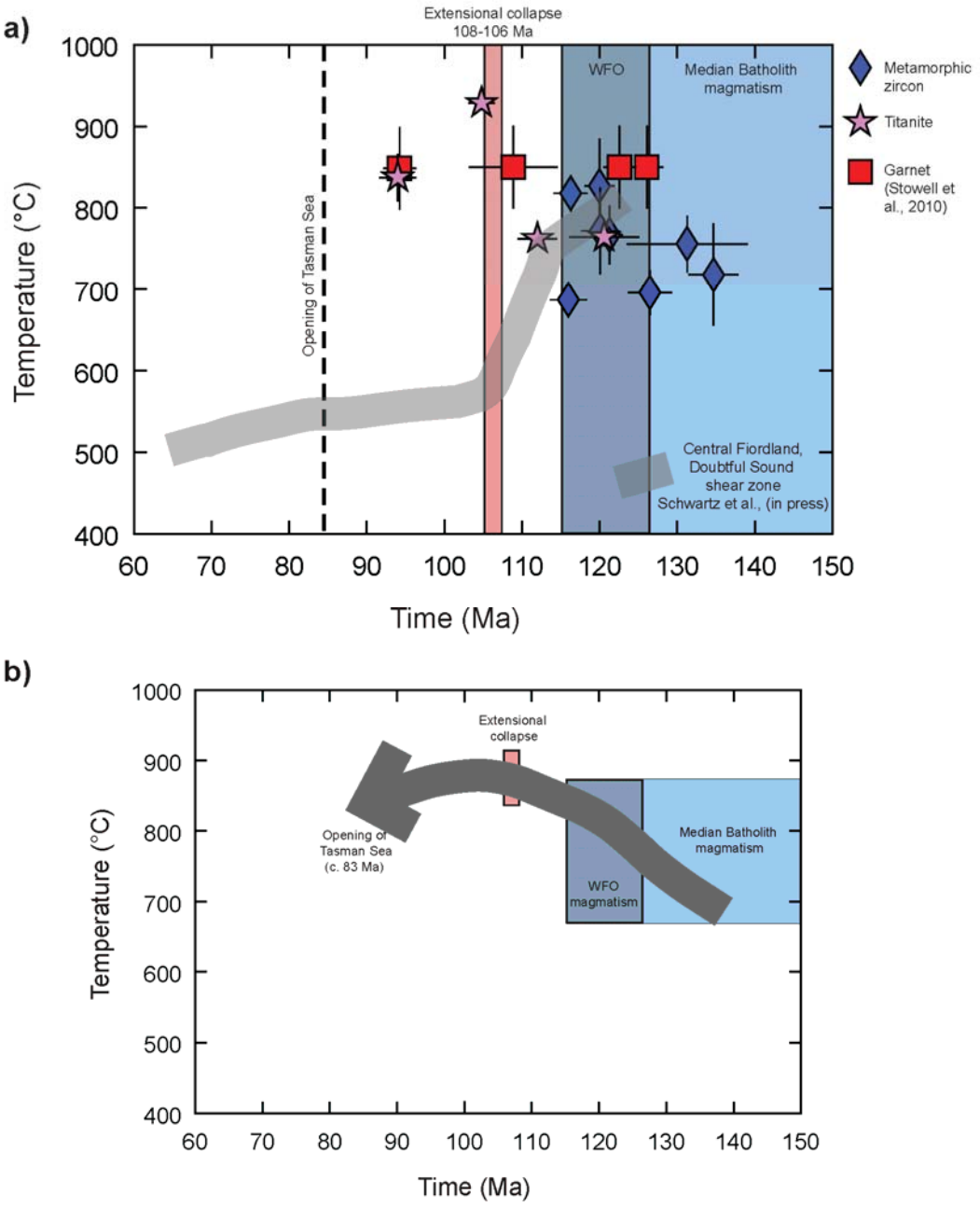

Figure 11: a) Time-temperature plot of metamorphic zircon (blue diamond), titanite (purple star), and Sm-Nd garnet (red box) dates and temperatures for northern Fiordland plotted against central Fiordland cooling curve from Schwartz et al. (in press); garnet data from Stowell et al. (2010). b) Time-temperature path for data from this study, including timing of major magmatic and tectonic events in Fiordland. Timing for Median Batholith magmatism indicated by light blue box; within Median Batholith magmatism, duration of WFO magmatism indicated by darker blue box. Initiation of extensional collapse designated by light blue box (108-106 Ma; Schwartz et al., in press. Opening of Tasman Sea indicated by dashed line (c. 84 Ma).

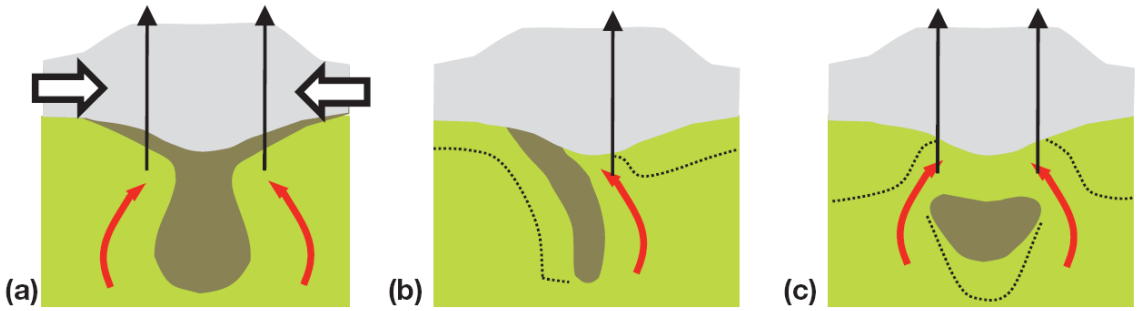

Figure 12: Scenarios in which foundering can occur in the lower crust. A) A Rayleigh-Taylor type instability. B) Delamination of a mafic lower crust root. C) Other type of delamination of a mafic lower crust root. Modified from Lee (2014).

6. CONCLUSION

U-Pb zircon and titanite thermochronology from northern Fiordland elucidates a protracted history of cooling and metamorphism associated with emplacement of the WFO during the last stage of Median Batholith magmatism. Metamorphic zircon record pre-WFO metamorphism occurring in the Arthur River Complex from 134.9 to 126.5 Ma and 756 – 696 °C; this corresponds to a granulite-facies metamorphic event recorded by Sm-Nd garnets (c. 134 Ma – 126 Ma, ~850 °C; Stowell et al., 2010) likely caused by tectonic accretion and/or partial melting (Daczko et al., 2002). During the emplacement of the WFO (c. 125-115 Ma), metamorphic zircons, and one titanite sample, record dates of 121.3 to 116.0 Ma at temperatures between 827 – 690 °C. These dates and temperatures illustrate high-temperature metamorphism taking place as a direct result of heat related to WFO intrusion into the mid to lower crust and its subsequent burial during tectonic collision. After the final pulse of Median Batholith magmatism, the growth / (re) crystallization of titanite grains record sustained high temperatures persisting in the lower crust between 112.0 and 94.0 Ma at temperatures between 928 and 753 °C.

Heat in the lower crust is primarily sustained at least partially through fluid migration in shear zones in central Fiordland; however, northern Fiordland lacks comparable extensional features and thus its protracted temperatures must be sustained through other means. Possible mechanisms which sustain heat in the lower crust in northern Fiordland include asthenospheric upwelling from a foundering dense root, heat sustained during a change in tectonic environment from convergence to extension, and/or basaltic diking and fracturing transmitting heat into the lower crust by extensional features not observed here. Together, these data from northern Fiordland confirm a

history of > 40 Ma of sustained heat and protracted cooling in the lower crust that mirrors that observed in central Fiordland. Further work is needed to constrain the mechanisms of protracted heating in northern Fiordland, such as further research into the foundering of a dense arc root, as well as examining extensional structure features which recorded extensional orogenic collapse in the region. Additionally, a study which utilizes U-Pb rutile and/or apatite thermochronology would complete the cooling history of the arc during and after regional extension. Ultimately, these methods of obtaining time-temperature data from zircon and titanite, as well as other accessory phases, can be accurately applied to other exposures of lower crust on Earth to further understand the timescales over which arcs remain hot and the means by which they do so.

REFERENCES CITED

Aleinikoff, J.N., Wintsch, R.P., Tollo, R.P., Unruh, D.M., Fanning, C.M., and Schmitz, M.D., 2007, Ages and origins of rocks of the Killingworth Dome, south-central Connecticut: implications for the tectonic evolution of southern New England, American Journal of Science, v. 307, p. 63-118.

Allibone, A.H., Jongens, R., Turnbull, I.M., Milan, L.A., Daczko, N.R., De Paoli, M.C., Tulloch, A.J., 2009, Plutonic rocks of western Fiordland, New Zealand: field relations, geochemistry, correlation, and nomenclature. New Zealand Journal of Geology and Geophysics, v. 52, p. 379-415.

Annen, C., Blundy, J.D., Sparks, R.S.J., 2006, The genesis of intermediate and silicic magmas in deep crustal hot zones. Journal of Petrology, v. 47, no. 3, p. 505-539.

Barth, A.P. and Wooden, J.L., 2010, Coupled elemental and isotopic analyses of polygenetic zircons from granitic rocks by ion microprobe, with implications for melt evolution and the source of granitic magmas. Chemical Geology, v. 277, p. 149-159.

Black, L.P., Kamo, S.L., Allen, C.M., Davis, D.W., Aleinikoff, J.N., Valley, J.W., Mundil, R., Campbell, I.H., Korsch, R.J., Williams, I.S., and Foudoulis, C., 2004, Improved $^{206}Pb/^{238}U$ microprobe geochronology by the monitoring of a trace-element-related matrix effect; SHRIMP, ID–TIMS, ELA–ICP–MS and oxygen isotope documentation for a series of zircon standards. Chemical Geology, v. 205, p. 115-140.

Bradshaw, J.Y., 1989, Origin and metamorphic history of an Early Cretaceous polybaric granulite terrain, Fiordland, southwest New Zealand. Contributions to Mineralogy and Petrology, v. 103, p. 346-360.

Bradshaw, J.Y., 1990, Geology of crystalline rocks of northern Fiordland: Details of the granulite facies Western Fiordland Orthogneiss and associated rock units. New Zealand Journal of Geology and Geophysics, v. 33, no. 3, p. 465-484.

Chapman A.D., Saleeby, J.B., Eiler, J., 2013, Slab flattening trigger for isotopic disturbance and magmatic flare-up in the southernmost Sierra Nevada batholith, California. Geology, v. 41, no. 9, p. 1007-1010.

Cherniak, D.J., 2010, Diffusion in accessory minerals: zircon, titanite, apatite, monazite, and xenotime. Reviews in Mineralogy and Geochemstry, v. 72, no. 1, p. 827-869.

Clarke, G.L., Klepeis, K.A., Daczko, N.R., 2000, Cretaceous high-P granulites at Milford Sound New Zealand: metamorphic history and emplacement in a convergent margin setting. Journal of Metamorphic Geology, v. 18, p. 359-374.

Corfu, F., Hanchar, J.M., Hoskin, P.W.O., Kinny, P., 2003, Atlas of zircon textures. Reviews in Mineralogy and Geochemistry, v. 53, no. 1, p. 469-500.

Daczko, N.R., Clarke, G.L., Klepeis, K.A., 2002, Kyanite-paragonite-bearing assemblages, northern Fiordland, New Zealand: rapid cooling of the lower crustal root to a Cretaceous magmatic arc. Journal of Metamorphic Geology, v. 20, no. 90, p. 887-902.

Daczko, N.R., Halpin, J.A., 2009, Evidence for melt migration enhancing recrystallization of metastable assemblages in mafic lower crust, Fiordland, New Zealand. Journal of Metamorphic Geology, v. 27, p. 167-185.

Davy, B., Hoernle, K., Werner, R., 2008, Hikurangi Plateau: Crustal structure, rifted formation, and Gondwana subduction history. Geochemistry, Geophysics, Geosystems, v. 9, no. 7, p. 1-31.

De Silva, S.L., Riggs, N.R., Barth, A.P., 2015, Quickening the Pulse: Fractal Tempos in Continental Arc Magmatism. Elements, v. 11, p. 113-118.

Ducea, M., 2001, The California arc: thick granitic batholiths, eclogitic residues, lithospheric-scale thrusting, and magmatic flare-ups. GSA Today, p. 4-10.

Dufek, J., Bergantz, G.W., 2005, Lower crustal magma genesis and preservation: a stochastic framework for the evaluation of basalt-crust interaction. Journal of Petrology, v. 46, no. 11, p. 2167-2195.

Flowers, R.M., Bowring, S.A., Tulloch, A.J., Klepeis, K.A., 2005, Tempo of burial and exhumation within the deep roots of a magmatic arc, Fiordland, New Zealand. Geology, v. 33, no. 1, p. 17-20.

Gibson, G.M., McDougall, I., Ireland, T.R., 1988, Age constraints on metamorphism and the development of a metamorphic core complex in Fiordland, southern New Zealand. Geology, v. 16, p. 405-408.

Hayden, L.A., Watson, E.B., Wark, D.A., 2008, A thermobarometer for sphene (titanite). Contributions to Mineralogy and Petrology, v. 155, p. 529-540.

Hildreth, W., Moorbath, S., 1988, Crustal contributions to arc magmatism in the Andes of Central Chile. Contributions to Mineralogy and Petrology, v. 98, p. 455-489.

Hollis, J.A., Clarke, G.L., Klepeis, K.A., Daczko, N.R., Ireland, T.R., 2003, Geochronology and geochemistry of high-pressure granulites of the Arthur River Complex, Fiordland, New Zealand: Cretaceous magmatism and metamorphism on the palaeo-Pacific Margin. Journal of Metamorphic Geology, v. 21, p. 299-313.

Hollis, J.A., Clarke, G.L., Klepeis, K.A., Daczko, N.R., Ireland, T.R., 2004, The regional significance of Cretaceous magmatism and metamorphism in Fiordland, New Zealand, from U-Pb zircon geochronology. Journal of Metamorphic Geology, v. 22, p. 607-627.

Ireland, T.R., and Williams, I.S., 2003, Considerations in zircon geochronology by SIMS. Reviews in Mineralogy and Geochemistry, v. 53, p. 215-241 (Hanchar JM and Hoskin WO, editors).

Klepeis, K.A., Clarke, G.L., Rushmer, T., 2003, Magma transport and coupling between deformation and magmatism in the continental lithosphere. GSA Today, v. 13, no. 1, p. 4-11.

Klepeis, K.A., Clarke, G.L., Gehrels, G., Vervoort, J., 2004, Processes controlling vertical coupling and decoupling between the upper and lower crust of orogens: results from Fiordland, New Zealand. Journal of Structural Geology, doi:10.1016/j.jsg.2003.08.012.

Klepeis, K.A., King, D., De Paoli, M., Clarke, G.L., 2007, Interaction of strong lower and weak middle crust during lithospheric extension in western New Zealand. Tectonics, v. 26, TC4017, doi:10.1029/2006TC002003, 2007.

Klepeis, K.A., Schwartz, J.J., Stowell, H., Tulloch, A., 2016, Gneiss domes, vertical and horizontal mass transfer, and the initiation of extension in the hot lower-crustal root of a continental arc, Fiordland, New Zealand. Lithosphere, doi:10.1130/L490.1.

Kylander-Clark, A.R.C., Hacker, B.R., Mattinson, J.M., 2008, Slow exhumation of UHP terranes: Titanite and rutile ages of the Western Gneiss Region, Norway. Earth and Planetary Science Letters, v. 272, p. 531-540.

Kylander-Clark, A.R.C., Hacker, B.R., Cottle, J.M., 2013, Laser-ablation split-stream ICP petrochronology. Chemical Geology, v. 345, p. 99-112.

Laird, M.G., Bradshaw, J.D., 2004, The Break-up of a Long-term Relationship: the Cretaceous Separation of New Zealand from Gondwana. Gondwana Research, v. 7, no. 1, p. 273-286.

Lee, C-T.A., 2014, "Physics and Chemistry of Deep Continental Crust Recycling." *Treatise on Geochemistry 2nd Edition.*

Ludwig, K.R., 2009, Squid 2, A user's manual, Berkeley Geochronology Center Special Publication No. 5, p. 110.

Ludwig, K.R., 2012, Isoplot 3.75, a geochronological toolkit for Excel, Berkeley Geochronology Center Special Publication No. 5, p. 75.

Marcotte, S.B., Klepeis, K.A., Clarke, G.L., Gehrels, G., Hollis, J.A., 2005, Intra-arc transpression in the lower crust and its relationship to magmatism in a Mesozoic magmatic arc. Tectonophysics, v. 407, p. 135-163.

Mattinson, J.M., Kimbrough, D.L., Bradshaw, J.Y., 1986, Western Fiordland orthogneiss: Early Cretaceous arc magmatism and granulite facies metamorphism, New Zealand. Contributions to Mineralogy and Petrology, v. 92, p. 383-392.

Mortimer, N., 2008, Zealandia. Arizona Geological Society Digest, v. 22, p. 227-234.

Mortimer, N., Rattenbury, M.S., King, P.R., Bland, K.J., Barrell, D.J.A., Bache, F., Begg, J.G., Campbell, H.J., Cox, S.C., Crampton, J.S., Edbrooke, S.W., Forsyth, P.J., Johnston, M.R., Jongens, R., Lee, J.M., Leonard, G.S., Raine, J.I., Skinner, D.N.B., Timm, C., Townsend, D.B., Tulloch, A.J., Turnbull, I.M., Turnbull, R.E., 2014, High-level stratigraphic scheme for New Zealand rocks, New Zealand Journal of Geology and Geophysics, v. 57, no. 4, p. 402-419.

Muir, R.J., Weaver, S.D., Bradshaw, J.D., Eby, G.N., Evans, J.A., 1995, The Cretaceous Separation Point batholith, New Zealand: granitoid magmas formed by melting of mafic lithosphere. Journal of the Geologic Society, London, v. 152, p. 689-701.

Nathan, S., Thurlow, C., Warnes, P., Zucchetto, R., 2000, Geochronology Database for New Zealand Rocks, 2nd edn. 1961-99. Institute of Geological and Nuclear Sciences report 2000/11, 51pp.

Paton, C., Hellstrom, J., Paul, B., Woodhead, J., and Hergt, J., 2011, Iolite: Freeware for the visualisation and processing of mass spectrometric data: Journal of Analytical Atomic Spectrometry, v. 26, p. 2508, doi: 10.1039/c1ja10172b.

Saleeby, J., Ducea, M., Clemens-Knott, D., 2003, Production and loss of high-density batholithic root, southern Sierra Nevada, California. Tectonics, v. 22, no. 6, 1064, doi:10.1029/2002TC001374.

Schwartz, J.J., Stowell, H.H., Klepeis, K.A., Tulloch, A.J., Kylander-Clark, A.R.C., Hacker, B.R., Coble, M.A., 2016, Thermochronology of extensional orogenic collapse in the deep crust, Fiordland, New Zealand. Geosphere (in press), doi:10.1130/GES1232.1.

Spencer, K.J., Hacker, B.R., Kylander-Clark, A.R.C., Andersen, T.B., Cottle, J.M., Stearns, M.A., Poletti, J.E., Seward, G.G.E., 2013, Campaign-style titanite U-Pb dating by laser-ablation ICP: Implications for crustal flow, phase transformations and titanite closure. Chemical Geology, v. 341, p. 84-101.

Stacey, J., and Kramers, J.D., 1975, Approximation of terrestrial lead isotope evolution by a two-stage model: Earth and Planetary Science Letters, v. 26, p. 207–221.

Stowell, H., Tulloch, A., Zuluaga, C., Koenig, A., 2010, Timing and duration of garnet granulite metamorphism in magmatic arc crust, Fiordland, New Zealand. Chemical Geology, v. 273, p. 91-110.

Tulloch, A.J., Ramezani, J., Mortimer, N., Mortensen, J., Van den Bogaard, P., Maas, P., 2009, Cretaceous felsic volcanism in New Zealand and Lord Howe Rise (Zealandia) as a precursor to final Gondwana break-up. Geological Society of London Special Publications, v. 321, p. 89-118.

Tulloch, A.J., Ireland, T.R., Kimbrough, D.L., Griffin, W.L., Ramezani, J., 2011, Autochthonous inheritance of zircon through Cretaceous partial melting of Carboniferous plutons: the Arthur River Complex, Fiordland, New Zealand. Contributions to Mineralogy and Petrology, v. 161, p. 401-421.

Whitney, D.L. and Evans, B.W., 2010, Abbreviations for names of rock-forming minerals. American Mineralogist, v. 95, p. 185-187.

Williams, I.S., 1997, U-Th-Pb geochronology by ion microprobe: not just ages but histories. Society Economic Geologists Rev. Econ. Geol., v. 7, p. 1-35.

APPENDIX A

Table DR1: SHRIMP-RG zircon isotopic analyses and ages. Uploaded as supplementary file due to size.

Table DR2: LASS-ICP-MS titanite isotopic analyses and ages. Uploaded as supplementary file due to size.

APPENDIX B

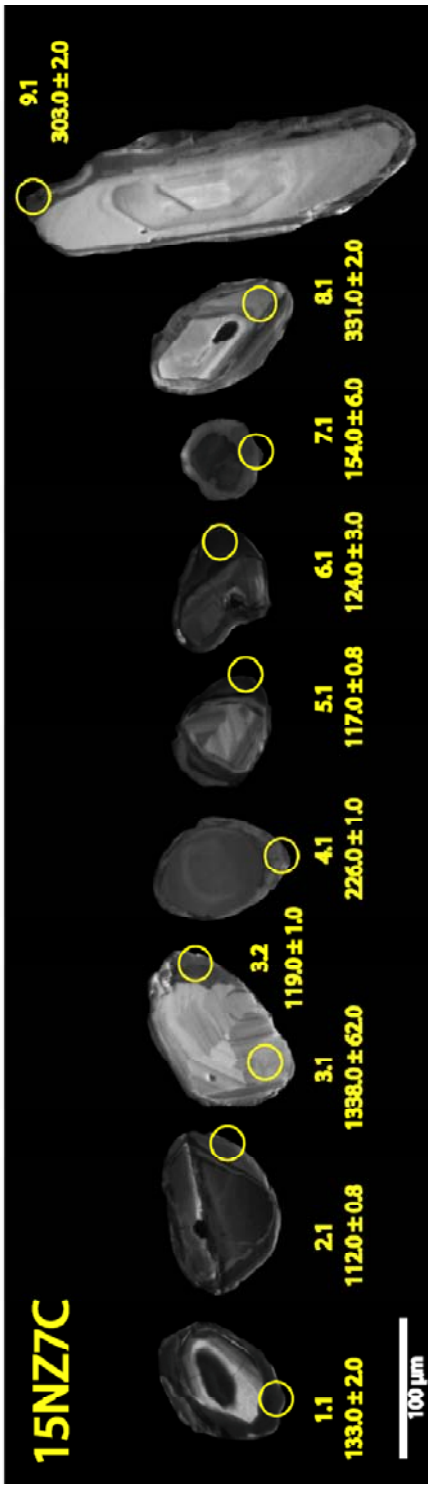

Figure DR3a: CL images of zircons from 15NZ7C.

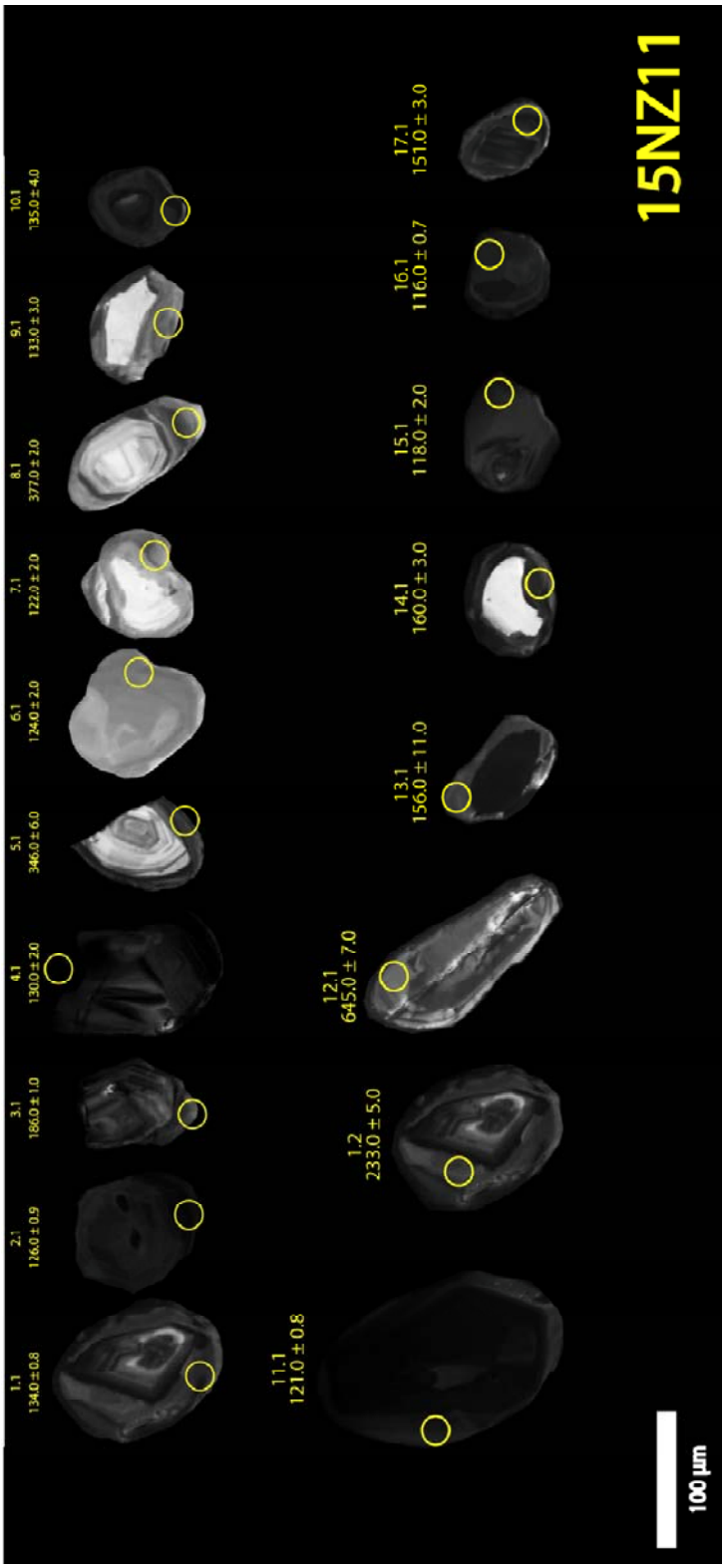

Figure DR3b) CL images of zircons from 15NZ11.

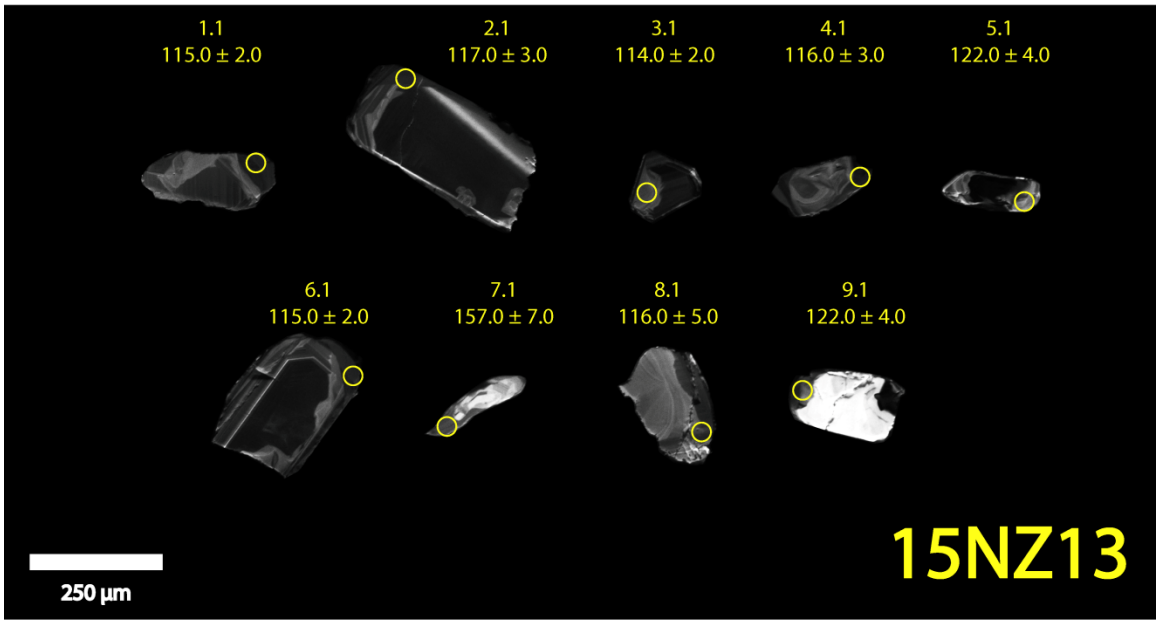

Figure DR3c) CL images of zircons from 15NZ13.

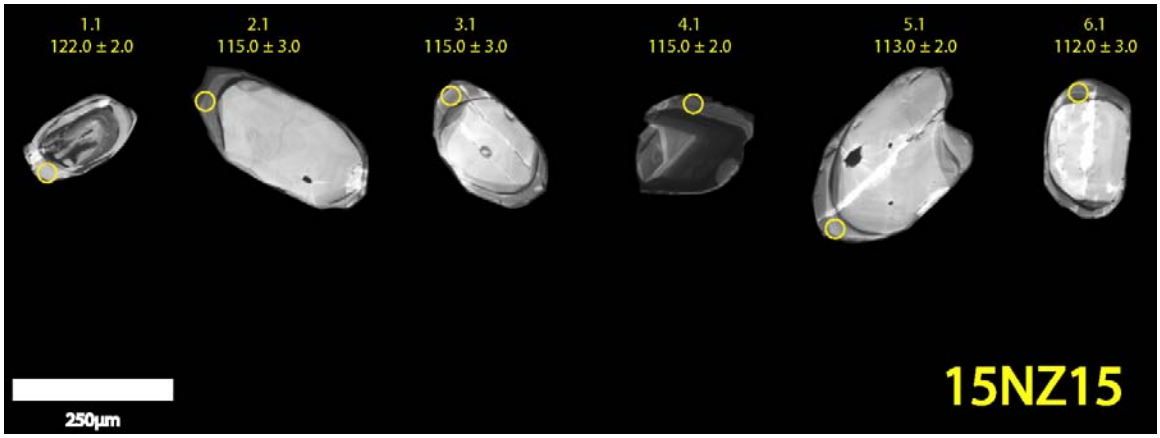

Figure DR3d) CL images of zircons from 15NZ15.

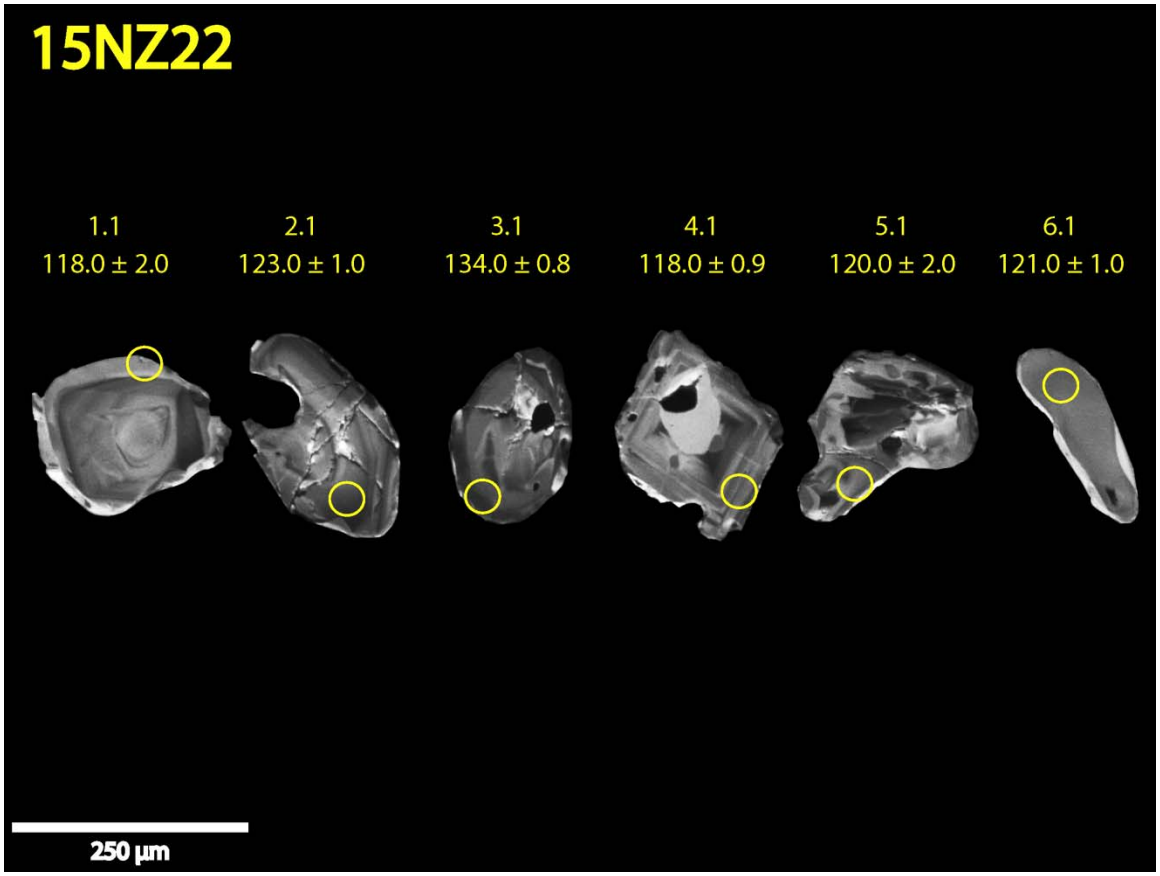

Figure DR3e) CL images of zircons from 15NZ22.

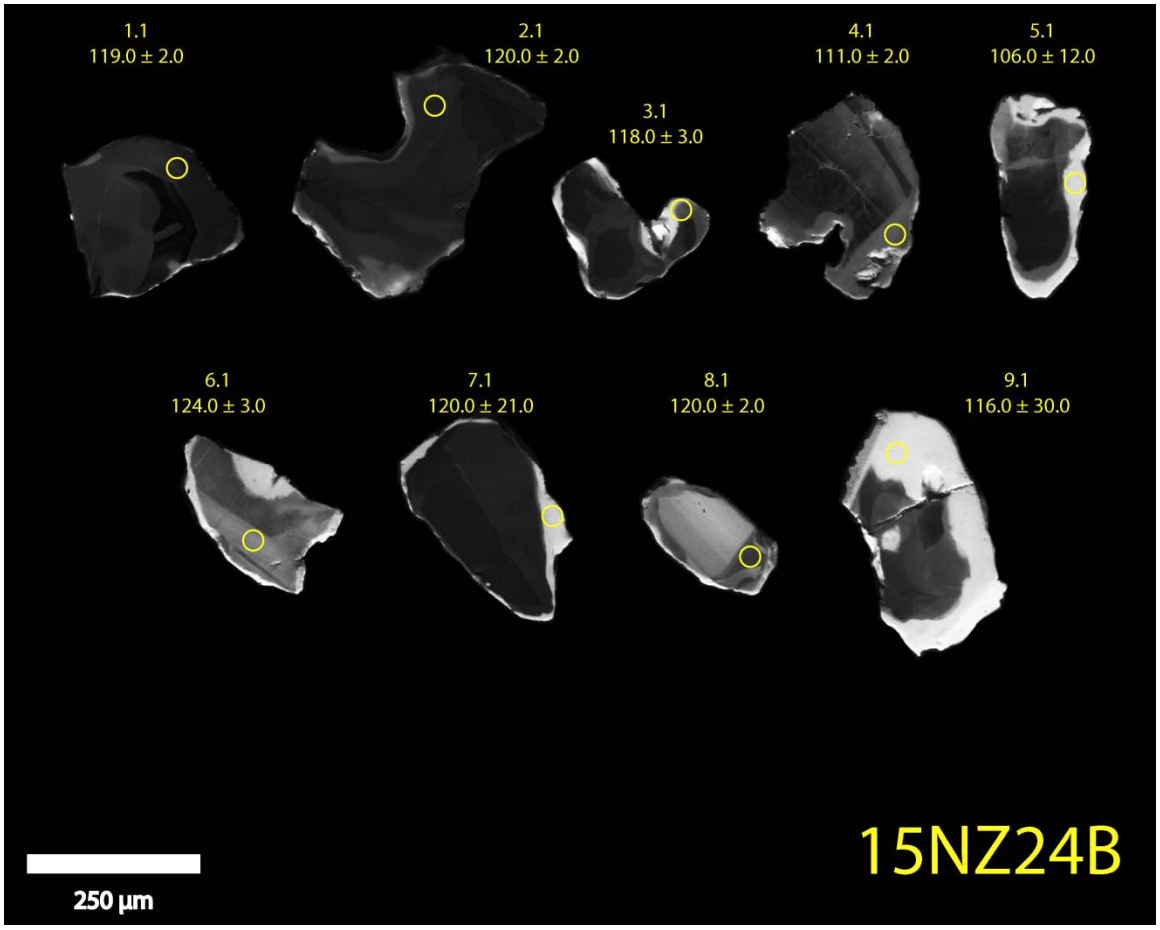

Figure DR3f) CL images of zircons from 15NZ24B.

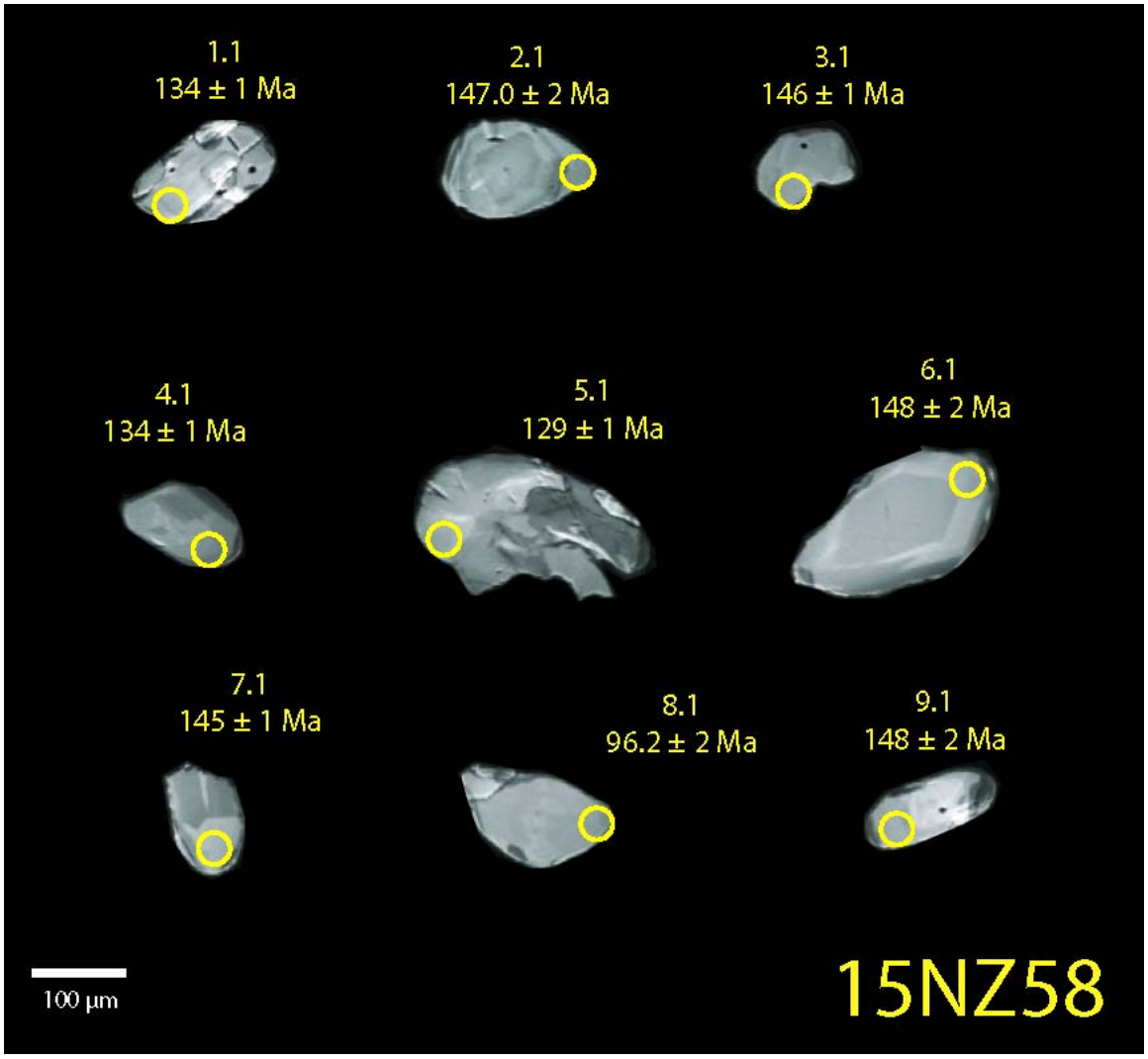

Figure DR3g) CL images of zircons from 15NZ58.

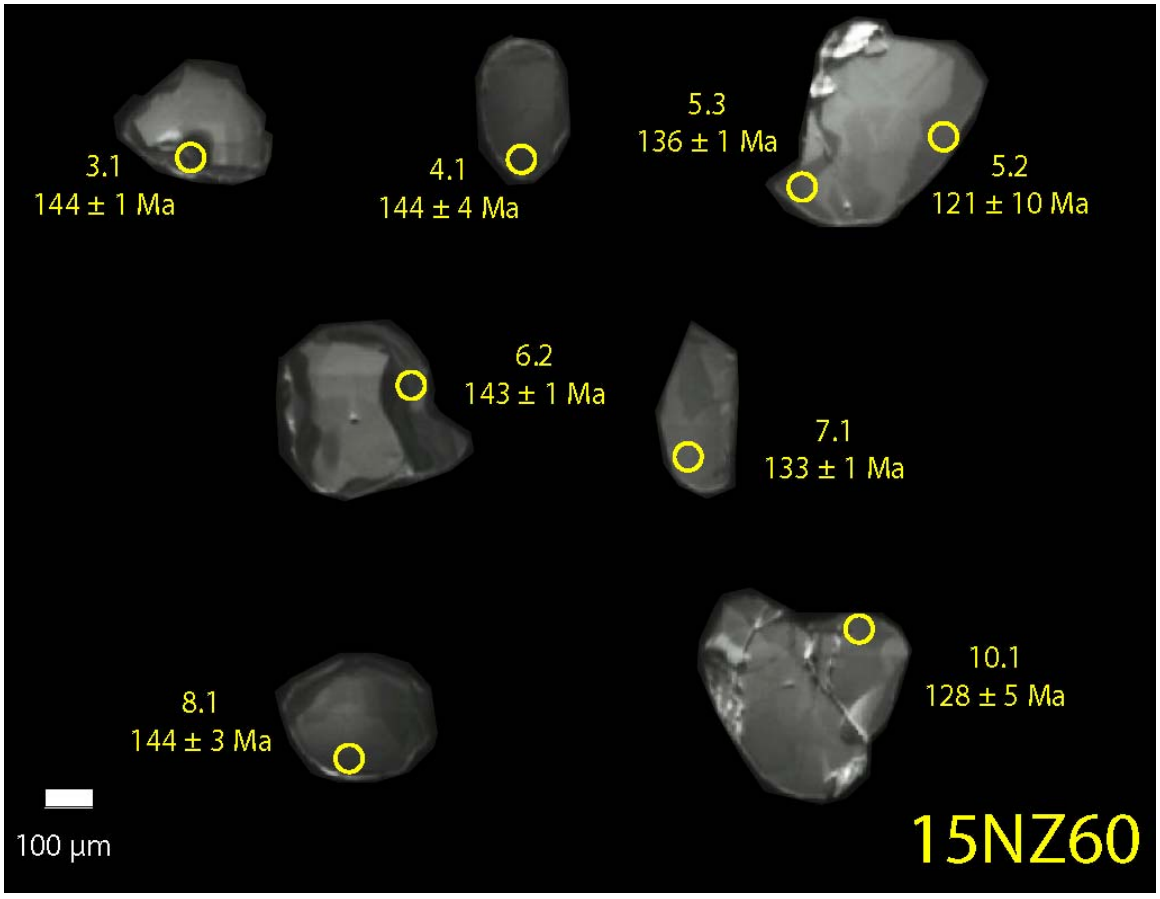

Figure DR3h) CL images of zircons from 15NZ60.

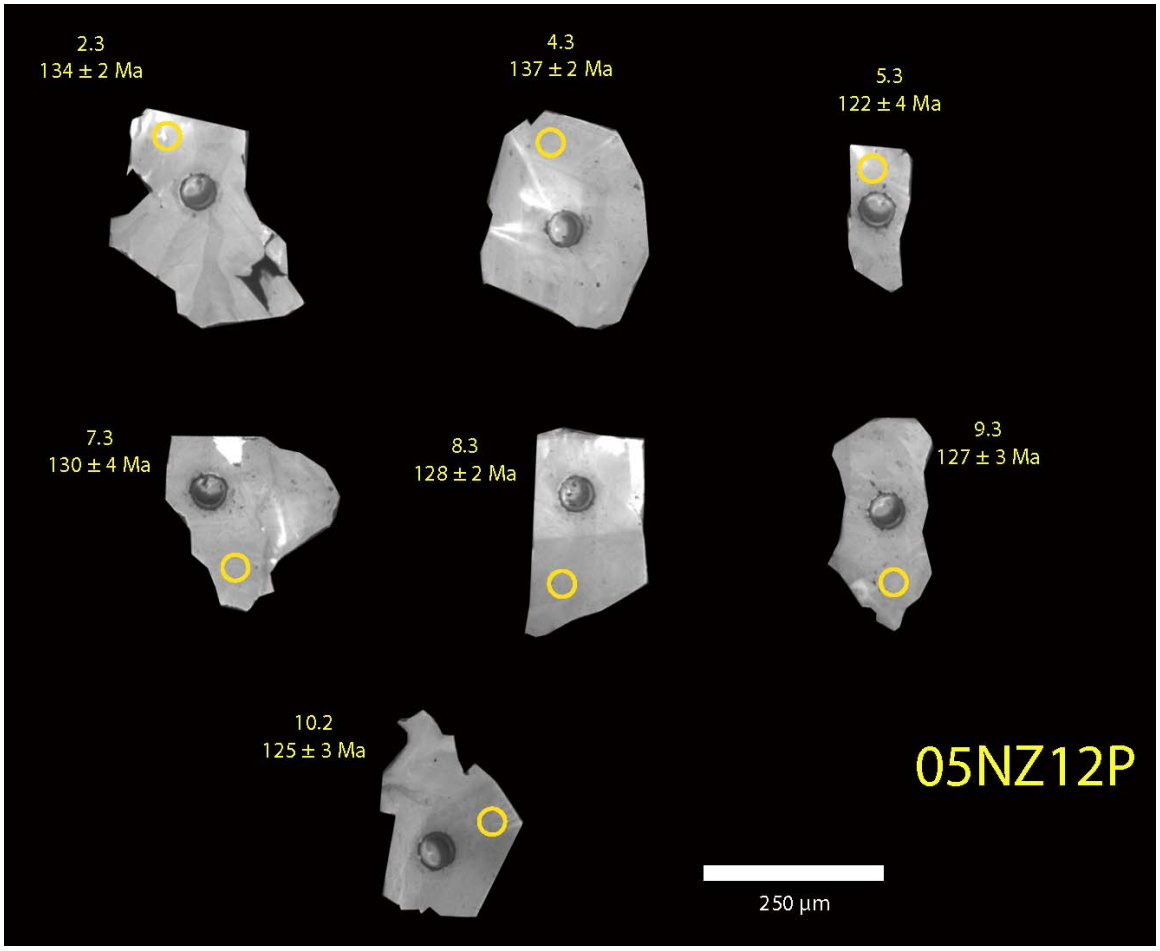

Figure DR3i) CL images of zircons from 05NZ12P.

APPENDIX C

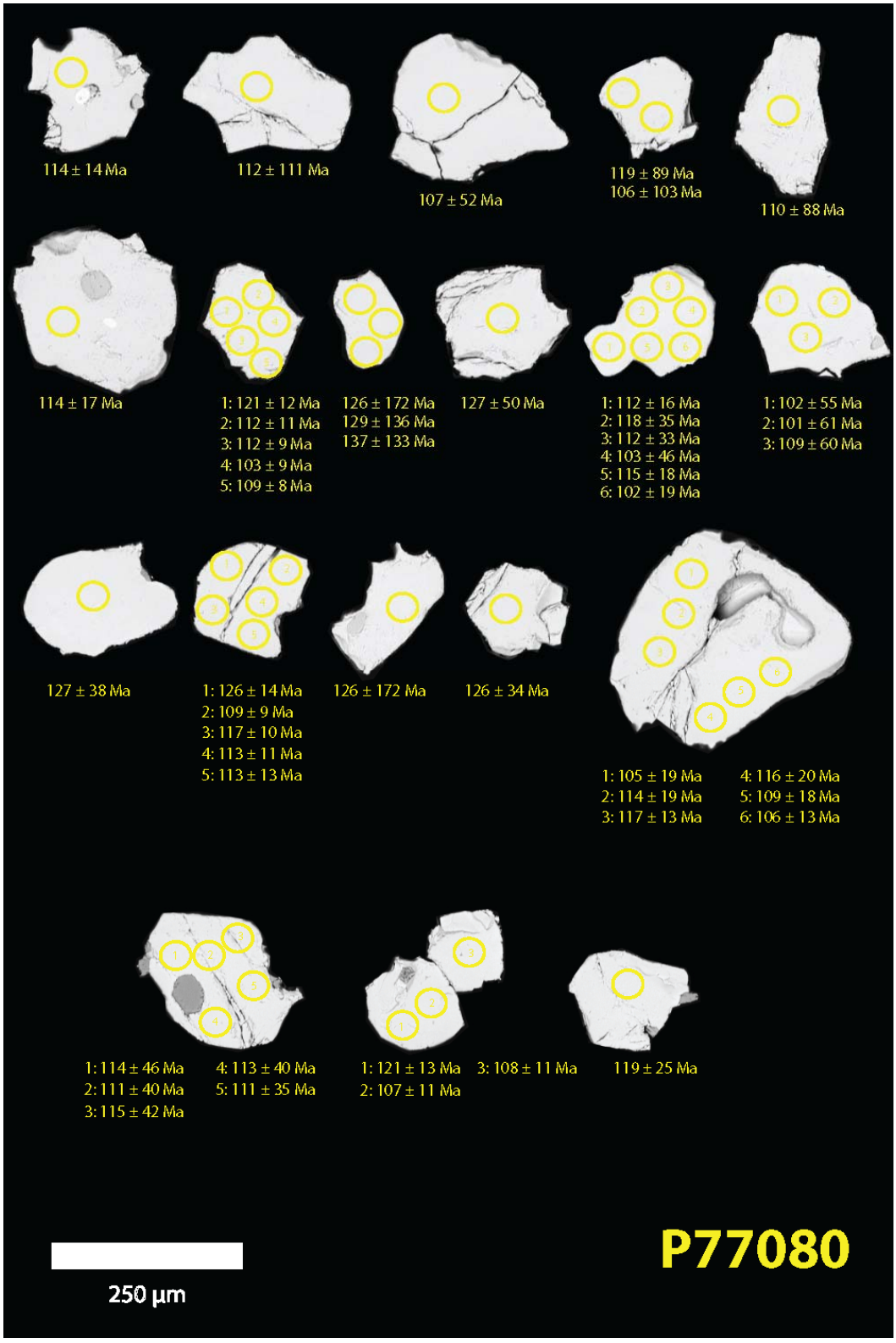

Figure DR4a) BSE images of titanite from sample P77080.

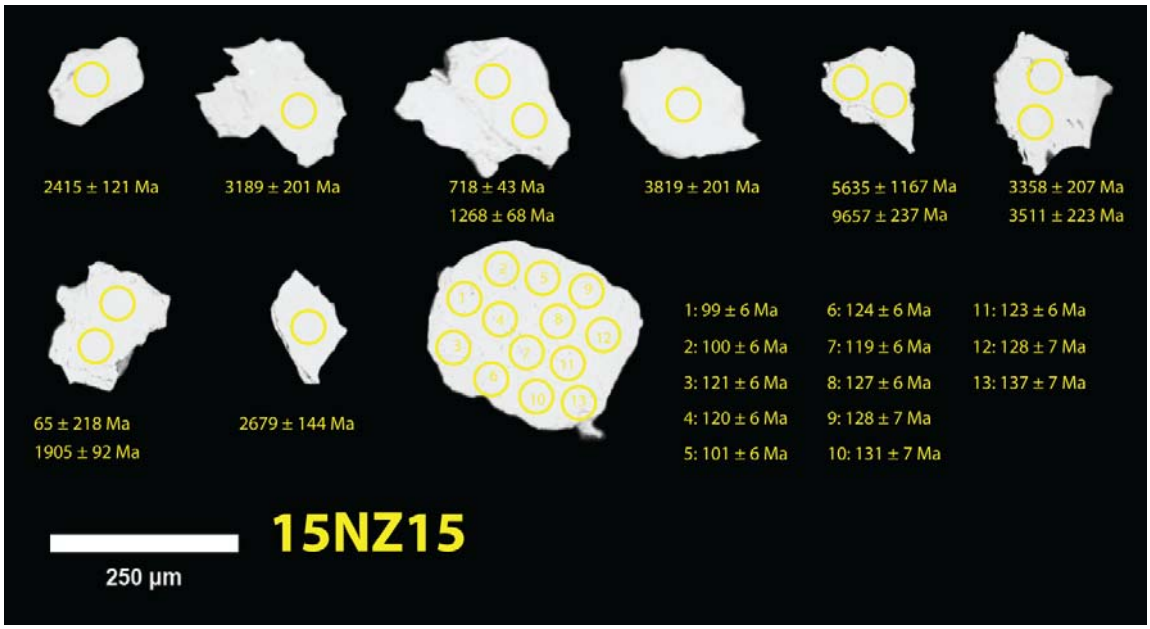

Figure DR4b) BSE images of titanite from sample 15NZ15.

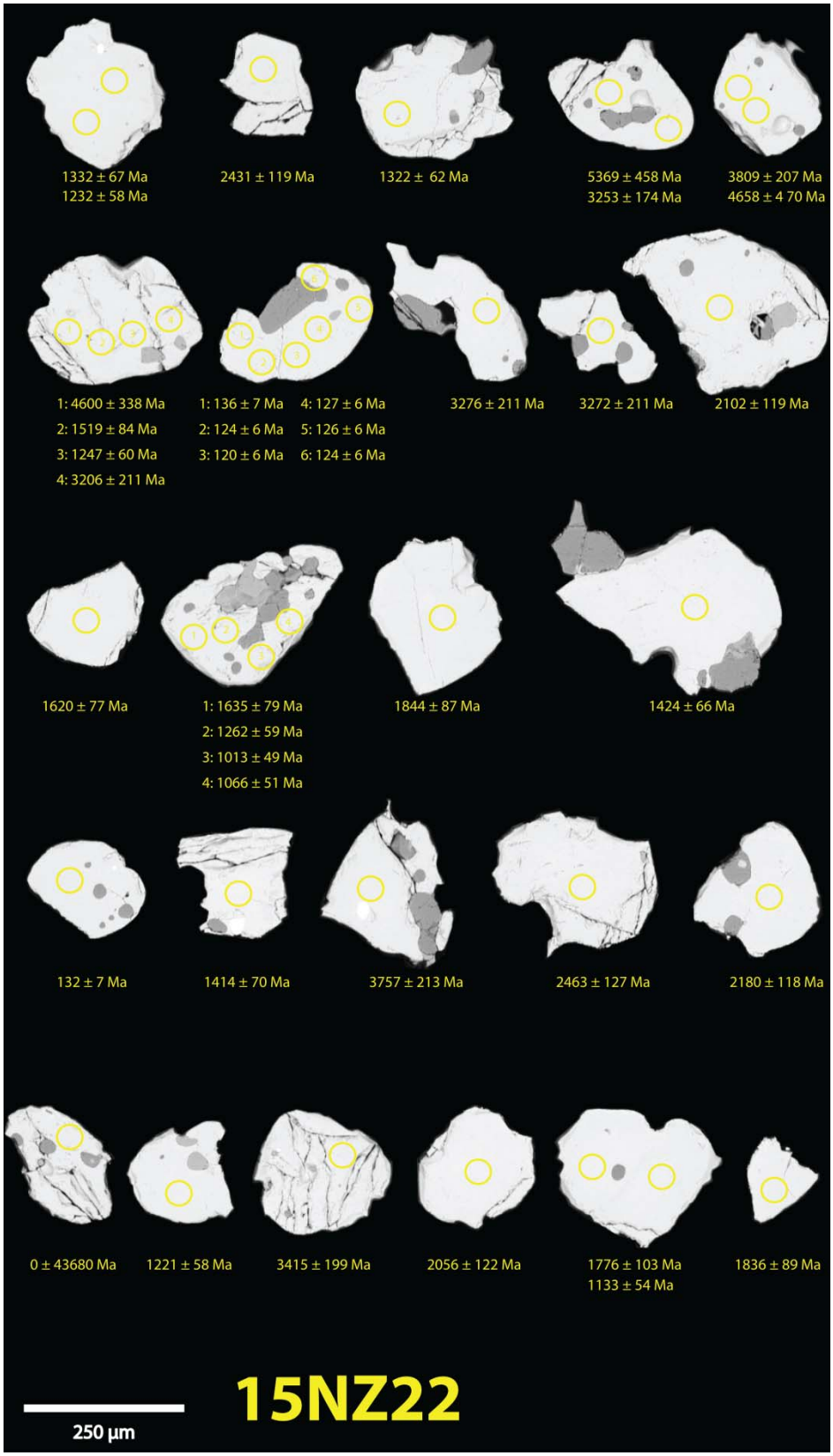

Figure DR4c) BSE images of titanite from sample 15NZ22.

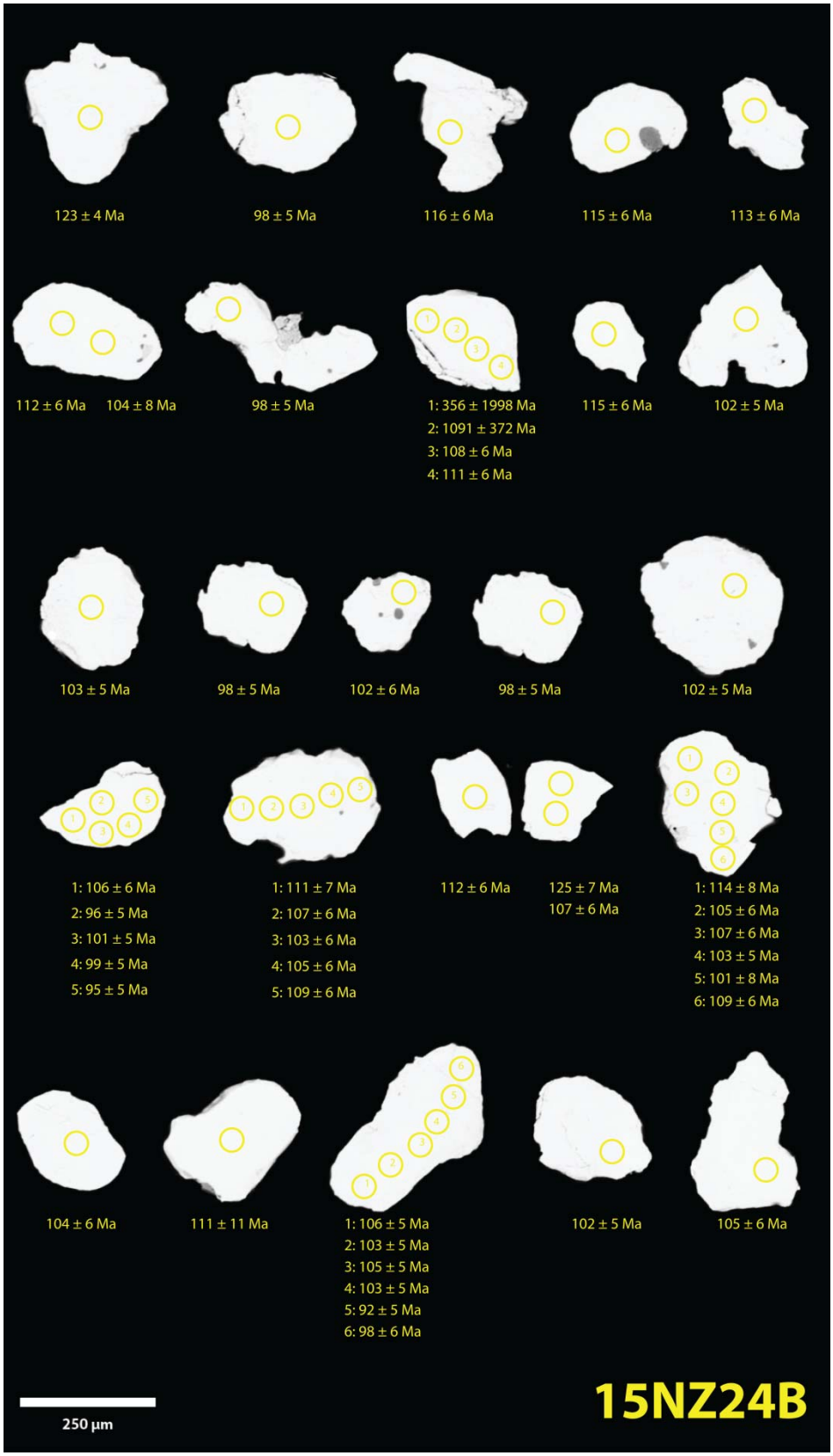

Figure DR4d) BSE images of titanite from sample 15NZ24B.

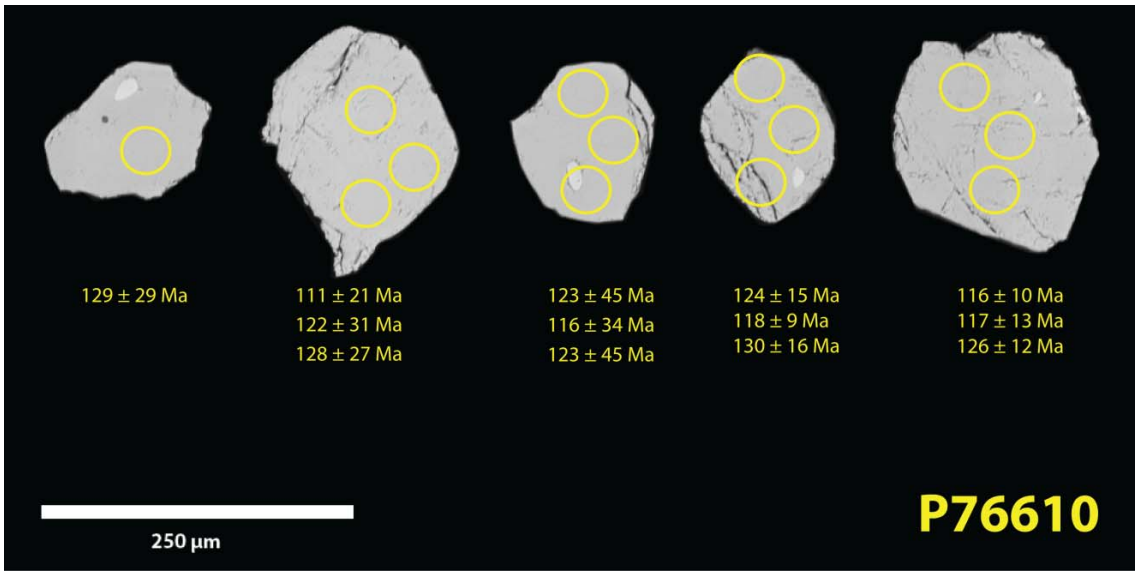

Figure DR4e) BSE images of titanite from sample P76610.

APPENDIX D

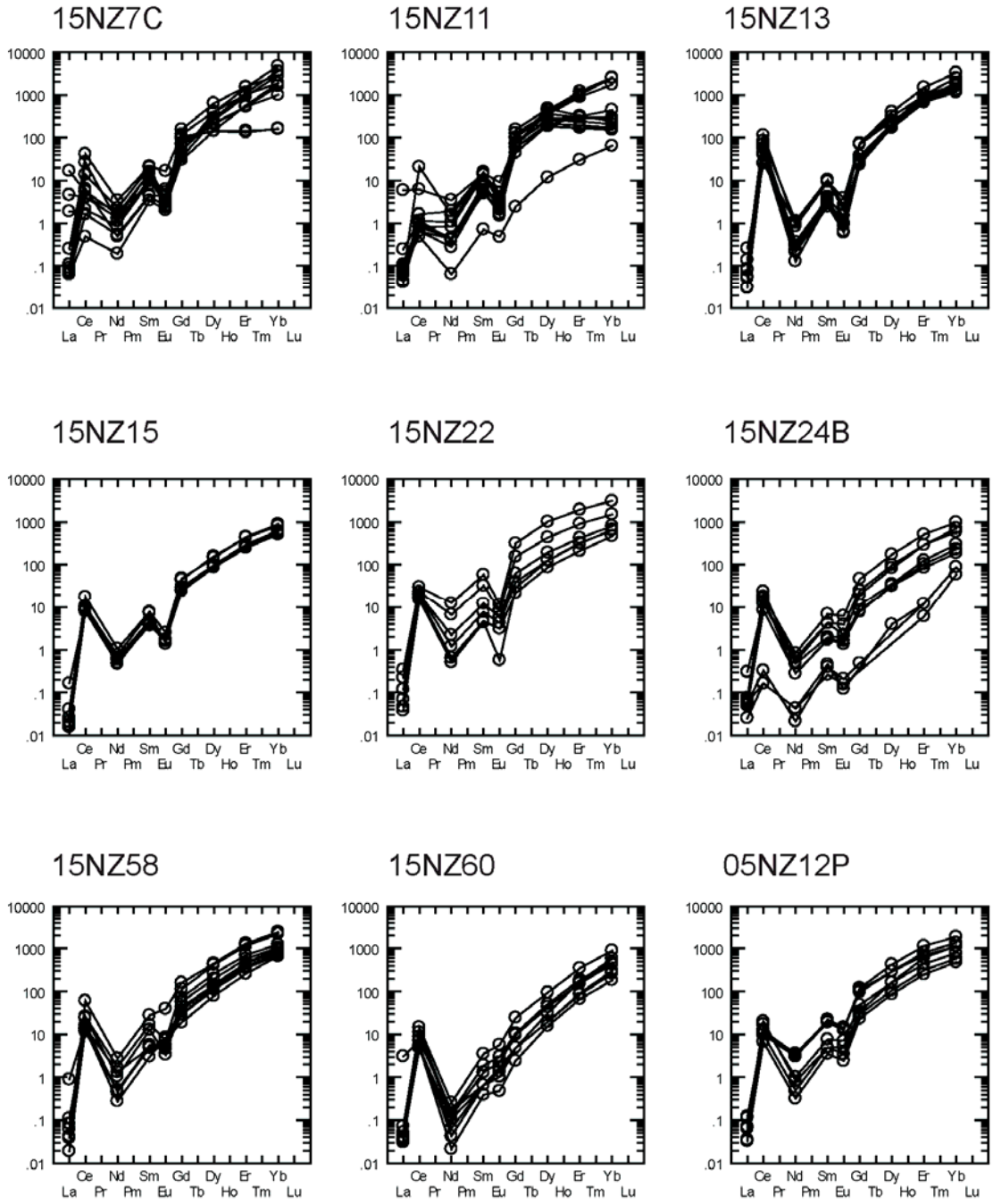

Figure DR5: Rare earth element spider diagrams.

APPENDIX E

Table DR6: Zircon trace element (REE) analyses, ppm, SHRIMP-RG. Uploaded as supplementary file due to size.

Table DR7: Titanite trace element (REE) analyses, ppm, LASS-ICP-MS. Uploaded as supplementary file due to size.